Decarbonizing urban public transport: development and final assessment of a hydrogen-fueled hybrid propulsion system for city buses

Fuel 420 (2026) 138866

Contents lists available at ScienceDirect

Fuel

journal homepage: www.elsevier.com/locate/fuel

Full Length Article

Decarbonizing urban public transport: development and final assessment of a hydrogen-fueled hybrid propulsion system for city buses

B. Peiretti Paradisi [a], F. Millo [a,*], L. Rolando [a], D. Di Battista [b], F. Di Prospero [b], E. Corti [c], P.P. Brancaleoni [c], M. Battistoni [d], J. Zembi [d], I. Arsie [e], A. Occhicone [e], M.R. Crispi [f]

[a] Energy Department, Politecnico di Torino, Italy
[b] Department of Industrial and Information Engineering and Economics, Università Dell'Aquila, Italy
[c] Department of Industrial Engineering, Università Degli Studi di Bologna, Italy
[d] Department of Engineering, Università Degli Studi di Perugia, Italy
[e] Department of Engineering, Università Degli Studi di Napoli Parthenope, Italy
[f] Department of Industrial Engineering, Università Degli Studi di Salerno, Italy

ARTICLE INFO

Keywords:
Decarbonization
H_2-ICE
Urban buses
Waste heat recovery
Energy management system
Hydrogen-SCR
Ultra-lean combustion

ABSTRACT

The H2ICE project focuses on the investigation of the feasibility and the development of a new class of hybrid powertrains incorporating a hydrogen-fueled Internal Combustion Engine (ICE) designed for 12-meter urban buses, with the goal of achieving low emissions and competitive efficiency. A combined experimental and simulation-based approach was adopted.

Achieving the full potential of this propulsion system requires significant advancements over the current state of the art, as several technical challenges remain. Chief among these is effectively managing the combustion process. First, a three-dimensional CFD model was calibrated and validated against an extensive optical-engine campaign, achieving predictive accuracy on mixture formation and flame development adequate for supporting design decisions in ultra-lean operation. This model supported the development of a complete one-dimensional engine model, coupled with a dedicated control strategy that improved combustion stability in the ultra-lean regime while enabling reduced NO_x formation and high efficiency.

Several Waste Heat Recovery (WHR) configurations were assessed through a synergy between experimental analysis and numerical simulations, including an electric turbocompound and an Organic Rankine Cycle (ORC). The combined two-stage WHR system achieved a maximum recovery efficiency of 14% (6.4% on average), delivering up to 16 kW of net electrical power under high exhaust energy conditions. In parallel, an innovative H_2-SCR concept was experimentally validated, reaching up to 50% NO_x conversion efficiency at exhaust temperatures around 250 °C and oxygen concentrations of approximately 12.5%.

A causal Rule-Based (RB) Energy Management System was designed as an implementable solution for real-time ECU application. In the final virtual-vehicle assessment over SORT driving cycles, hydrogen consumption reached values as low as 9 kg/100 km (i.e., meeting the project target of ~ 10 kg/100 km under standardized conditions), while real-world variability may lead to higher values, as discussed in the manuscript. Tailpipe NO_x emissions ranged from approximately 0.14 g/kWh under standardized type-approval cycles to as low as 0.009 g/kWh under real-world operating conditions, remaining below the forthcoming Euro 7 limits for heavy-duty applications.

These results demonstrate that H_2ICE-based hybrid powertrains represent a technically feasible and realistic solution for urban buses, capable of delivering low pollutant emissions and competitive efficiency, and offering a viable decarbonization pathway in contexts where battery-electric solutions face infrastructure or range limitations.

* Corresponding author.
E-mail addresses: benedetta.peiretti@polito.it (B. Peiretti Paradisi), federico.millo@polito.it (F. Millo), luciano.rolando@polito.it (L. Rolando), davide.dibattista@univaq.it (D. Di Battista), federico.diprospero@graduate.univaq.it (F. Di Prospero), enrico.corti2@unibo.it (E. Corti), pier.brancaleoni2@unibo.it (P.P. Brancaleoni), michele.battistoni@unipg.it (M. Battistoni), jacopo.zembi@unipg.it (J. Zembi), ivan.arsie@uniparthenope.it (I. Arsie), alessio.occhicone@uniparthenope.it (A. Occhicone), mcrispi@unisa.it (M.R. Crispi).

https://doi.org/10.1016/j.fuel.2026.138866
Received 9 September 2025; Received in revised form 17 February 2026; Accepted 19 February 2026
Available online 26 February 2026

Nomenclature

Acronyms and symbols

ATS	Aftertreatment System
BEV	Battery Electric Vehicle
BMEP	Brake Mean Effective Pressure
BSFC	Brake Specific Fuel Consumption
BTE	Brake Thermal Efficiency
CA50	Crank Angle of 50% Mass Fraction Burned
CFD	Computational Fluid Dynamics
DI	Direct Injection
DoE	Design of Experiment
ECU	Engine Control Unit
EG	Electric Generator
EGR	Exhaust Gas Recirculation
EMS	Energy Management System
FC	Fuel Consumption
FCEV	Fuel Cell Electric Vehicle
GHG	Green House Gas
HEV	Hybrid Electric Vehicle
HRVG	Heat Recovery Vapor Generator
ICE	Internal Combustion Engine
IMEP	Indicated Mean Effective Pressure
IT	Ignition Timing
LCA	Life Cycle Assessment
MAP	Manifold Absolute Pressure
MBT	Maximum Brake Torque
NO_x	Nitrogen Oxides
ORC	Organic Rankine Cycle
PFI	Port Fuel Injection
PMP	Pontryagin Minimum Principle
RB	Rule-Based
RMSE	Root Mean Square Error
RNG	Renormalization Group
SCR	Selective Catalytic Reduction
SiL	Software in the Loop
SV	Space Velocity
TC	Turbo Compound
TCO	Total Cost of Ownership
U-RANS	Unsteady Reynolds Averaged Navier-Stokes
WHR	Waste Heat Recovery
$c_{p,gas}$	Specific heat capacity of exhaust gas
C_{SCR}	SCR thermal capacity
h_{amb}	Convective heat-transfer coefficient SCR–ambient
h_{in}/h_{out}	Enthalpy of working fluid at component inlet/outlet
H	System Hamiltonian
$\dot{m}_{gas}$	Exhaust gas mass flow rate
$\dot{m}_{WF}$	Working-fluid mass flow rate in the ORC
NOx_{in}/NOx_{out}	Inlet/outlet NOx concentration in the SCR
P_{exp}/P_{pump}	Expander power / Pump power in ORC
$p_{in,TC}/p_{out,TC}$	Turbocompound inlet / outlet pressure
P_{TC}	Power delivered by the turbocompound
P_{ICE}	Power delivered by the ICE
m_{H2}	Hydrogen mass flow
P_{ORC}	Net ORC electrical power
$\dot{Q}_{RC}$	Thermal power recovered by HRVG in the ORC
S_L	Laminar flame speed
S_T	Turbulent flame speed
T_{exh}	Engine-out exhaust gas temperature
$T_{in,TC}/T_{out,TC}$	Turbocompound inlet / outlet gas temperature
T_{SCR}	SCR temperature
β	Turbocompound Expansion ratio ($p_{in,TC}$ / $p_{out,TC}$)
η_{TC}	Turbocompound adiabatic efficiency
η_{EM}	Electromechanical efficiency
η_{SCR}	SCR conversion efficiency
η_{WHR}	Overall WHR efficiency
λ	Relative air-to-fuel-ratio

1. Introduction

The decarbonization of urban public transport represents a critical challenge in the global effort to address climate change and mitigate the health impacts of air pollution. Diesel-powered bus fleets, while long established as the backbone of city mobility, contribute significantly to greenhouse gas (GHG) emissions and urban air pollutants. Recent efforts have therefore focused on alternative propulsion systems, including battery electric vehicles (BEVs) and low-carbon fuel solutions; however, large-scale BEV deployment may be limited by infrastructure readiness, electricity availability and local operational constraints [1].

Hydrogen stands out among alternative fuels due to its carbon-free molecular structure, which ensures zero tailpipe CO_2 emissions in both fuel cell electric vehicles (FCEVs) and hydrogen internal combustion engines (H_2-ICEs) [2]. While policy attention has mainly targeted FCEVs and BEVs, H_2-ICEs provide a promising intermediate option for medium- and heavy-duty transport, especially where driving range, payload and operational flexibility are critical [3]. H_2-ICEs maintain the advantages of the conventional ICE platform and emit only water vapor during ideal combustion conditions, although high temperatures can still generate NO_x. Experimental work indicates that NO_x formation is strongly affected by mixture preparation, combustion phasing and turbocharged operation [4], highlighting the necessity of coordinated combustion and After-Treatment System (ATS) optimization. Moreover, ultra-lean hydrogen combustion, an essential operating mode for high efficiency, poses challenges related to mixture formation, ignition stability and increased sensitivity to in-cylinder thermodynamic conditions [5]. Validated CFD tools for these regimes are still limited, underscoring the need for experimental data and system-level validation to support model development.

Beyond emissions, H_2-ICEs offer logistical and economic advantages when compared with BEVs and FCEVs. They are compatible with existing manufacturing lines, maintenance practices, and service infrastructure, which lowers the barrier to large-scale adoption. Technologically, they require less complex systems than FCEVs, avoiding the need for fuel cell stacks and their associated thermal management challenges [6].

A further advantage is the potential to retrofit existing diesel ICEs to operate on hydrogen. This approach can reduce capital expenditures and facilitate early transitions in public transport fleets without necessitating entirely new vehicle platforms. Recent developments by manufacturers such as Mahle [7] and Phinia [8] have demonstrated the feasibility of this retrofit strategy. Such solutions are particularly relevant for transit agencies facing tight budget constraints and operating vehicles with long lifecycles. Hybrid H_2-ICE powertrains can also deliver additional benefits: recent studies have shown that integrating hydrogen combustion with hybridization can reduce the energy consumption of a diesel bus by an average of 29% [9]. This aligns with previous work on hybrid bus development, which highlights how hybridization can compensate for engine limitations in transient urban driving conditions [10]. However, integrating additional subsystems such as waste heat recovery (WHR) units and hydrogen-compatible SCR technologies introduces further challenges, including exhaust thermal management, component packaging and control strategy coordination, especially under highly variable urban cycles.

Life Cycle Assessment (LCA) provides a broader view of

environmental performance. BEVs achieve low use-phase emissions when powered by renewable electricity [11], but their overall impact depends on several boundary conditions such as: grid carbon intensity, battery production burdens and diverse weather conditions [12]. The environmental profile of H_2-ICE buses similarly depends on the hydrogen pathway, with green hydrogen offering substantial GHG reductions [13]. Comparative LCAs consistently show that BEV and H_2-ICE solutions present context-dependent advantages driven by energy supply and manufacturing processes [6,11], underscoring the need for system-level analysis.

Economic viability must also be considered. BEVs often yield favorable TCO due to high efficiency and low maintenance, but limitations such as upfront costs, range constraints and charging requirements may restrict their adoption under demanding operating conditions [14]. H_2-ICEs may offer greater operational flexibility, especially in regions where hydrogen infrastructure already exists or is being planned and can achieve competitive cost performance relative to FCEVs. Scenario-based studies on hydrogen mobility confirm that cost-effectiveness, together with good environmental performance, strongly depends on energy market and infrastructure evolution, reinforcing the need to assess propulsion technologies within realistic boundary conditions [13].

Although real-world applications remain relatively limited, they are steadily increasing. Pilot programs in the European Union and California [15,16] have introduced H_2-ICE buses, often as part of broader hydrogen mobility initiatives. These initiatives demonstrate the feasibility of hydrogen mobility but also highlight the need for advances in fuel injection systems, turbocharging strategies and engine management. Hybridization remains a promising pathway for improving efficiency and emissions performance in urban applications [10]. Despite these contributions, most existing studies assess combustion behavior, ATS performance, hybridization strategies or environmental impacts separately [4–16]. Limited work has combined ultra-lean combustion behavior, WHR integration, H_2-SCR operation and hybrid controls into a unified framework. As a result, system-level understanding of their combined influence on NO_x reduction, conversion efficiency and vehicle-level performance remains incomplete.

In this context, the present paper focuses on the final results of the H_2ICE project, a research and demonstration program aimed at evaluating the technical feasibility, operational performance, and integration challenges of hydrogen-fueled internal combustion engines in public transport. Building on earlier publications that detailed the project's development phase [17], this work addresses the concluding assessment phase, covering both engine-level and system-level analyses. A new contribution of this study is the integrated evaluation of combustion behavior, WHR systems, and H_2-SCR aftertreatment within a hybrid bus platform, thereby addressing the knowledge gap identified above. The study provides insight into the capabilities and limitations of H_2-ICE buses in real-world transit scenarios and assesses their potential role alongside BEVs and other clean propulsion technologies in achieving sustainable urban mobility.

The paper is organized as follows: Section 2 presents an overview of the final achievements of the H_2ICE project, including the case study context and target performance metrics. Section 3 analyzes the combustion system, while Section 4 examines the waste heat recovery system and ATS solutions. Section 5 discusses engine and powertrain management strategies. Section 6 integrates these findings into a virtual vehicle assessment, and Section 7 concludes with the main outcomes and recommendations for future research.

2. H_2ICE overview and final goals

2.1. Case study

The considered vehicle is a 12-metric-ton urban bus employing a series hybrid architecture, integrating a hydrogen internal combustion engine derived from a state-of-the-art diesel engine and an electric traction motor as power sources [17]. Table 1 reports the main vehicle-level specifications used in this study, which are representative of a standard 12-m urban bus class widely adopted in European public transport fleets. The curb and fully loaded weights reflect typical operational conditions, considering both the structural mass and a full passenger load of approximately 90 people, which is standard for high-capacity urban buses. The road load values at 50, 80 and 100 km/h were derived from coast down-equivalent data from a similar vehicle architecture [10] and are consistent with the aerodynamic and rolling resistance characteristics of vehicles in this category.

The main powertrain components' technical specifications in Table 2. More details about the components' choice and sizing can be found in [17].

The design of the hybrid traction system considered both standardized regulatory driving cycles and representative real-world mission profiles. Specifically, three distinct mission profiles characteristic of typical urban bus operations are analyzed. Their corresponding speed profiles are illustrated in Fig. 1. Specifically, the Braunschweig cycle is an urban driving cycle commonly utilized in research studies and equipment certification programs [18]. The MLTB cycle, developed by UK transport authorities in 1996, serves to assess the compliance of new vehicles with emissions and fuel economy regulations [19]. Lastly, the Gillingham Uphill profile represents a real-world driving scenario derived from GPS data, characterized by significant elevation changes to evaluate vehicle performance under demanding operating conditions [20].

2.2. Main research areas and project targets

The H_2ICE project has been focused on advancing hydrogen-fueled ICE technology for integration into hybrid powertrains, particularly for use in urban buses. To unlock the full potential of hydrogen as a clean and efficient fuel, the initiative addressed several technical barriers by combining experimental development, simulation, and systems integration. Through this integrated approach, the project aimed to push the state of the art in hydrogen powertrain design, combustion control, and emissions reduction. Indeed, the main focus of the project has been divided into three main areas, as follows:

Combustion and fuel injection systems.

- Enhance computational modeling of hydrogen combustion and emissions.
- Expand experimental datasets on H_2 ignition and combustion under engine-relevant pressure and temperature conditions.
- Mitigate abnormal combustion such as surface ignition, backfiring, preignition, and knock due to H_2's reactive properties.

Waste Heat Recovery Technologies and Aftertreatment System.

- Develop advanced WHR systems to utilize high exhaust gas enthalpy for energy efficiency, tailored for the present application.
- Innovate a Selective Catalytic Reduction (SCR) system using hydrogen as the reductant to achieve near-zero tailpipe Nitrogen Oxides (NO_x).

Table 1
Hybrid bus specifications and target setting.

Vehicle length	12 m
Curb weight	12 ton
Fully loaded weight	18 ton
Full passenger capacity	90
Road Load @ 50 km/h	16 kW
Road Load @ 80 km/h	43 kW
Road Load @ 100 km/h	74 kW

Table 2
Hybrid powertrain technical specifications.

ICE	**Displacement**	3.0 L
	Bore × stroke	83 × 90 mm
	Features	Single stage Turbocharger w/VGT
	Max. power	100 kW
EM	**Max. power**	200 kW
	Max. torque	1500 Nm
Battery	**Capacity**	19.8 kWh
	Nominal voltage	396 V
	Maximum current	2400 A
	Maximum power	950 kW
	Cell in series	120
	Cell in parallel	20

- Design and test catalysts compatible with hydrogen-based ATS systems.
- Integrate and coordinate WHR and H_2-SCR systems for optimal emission control and thermal energy usage.

Engine and Hybrid Powertrain Management.

- Design of a combustion controller managing the control action to assure the requested torque production with optimal performance.
- Develop control strategies for the coordinated operation of WHR and SCR systems.
- Develop an Energy Management System (EMS) to improve the overall efficiency of hydrogen-powered hybrid systems.

Furthermore, Table 3 reports the overall targets adopted in this study, defined based on state-of-the-art evidence for turbocharged ultra-lean H_2 combustion and hybrid powertrain operation. The engine targets originate from the project's engineering goals, which identified ultra-lean operation as the key enabler for simultaneously achieving high efficiency and very low engine-out NO_x, to be further reduced by the H_2-SCR system. As an example, the peak ICE efficiency target of 42% reflects the values reported for boosted H_2 engines operating at $\lambda > 2$, where mixture formation, spark timing and elevated boost enable high thermodynamic efficiency while keeping pressure-rise rates low [4,21,22]. Similarly, the tailpipe NO_x target (<0.05 g/kWh) results from combining the inherently low-NO_x characteristics of ultra-lean combustion with the additional reduction achievable through H_2-SCR aftertreatment, consistent with the NO_x formation trends observed in experimental studies. The WHR and e-turbo efficiency targets (>4%) derive from the high exhaust gas enthalpy available, which makes waste heat recovery and turbocompounding viable contributors to overall system efficiency. Finally, the 10 kg/100 km hydrogen-consumption objective aligns with the system-level performance goals set within the H2ICE project and is consistent with the improvements observed in comparable hybrid bus prototypes [10]. These targets therefore provide coherent boundary conditions for component design, hybrid energy-management optimization and vehicle-level assessment.

3. Combustion system

Managing hydrogen injection and combustion poses challenges due to the risk of backfire in port injection and to the complexities of mixture formation in direct injection. In previous works related to the project [17,23–25] CFD models have been developed for investigating different injection options, from Port Fuel Injection (PFI) to Direct Injection (DI) with various nozzle designs, to assess mixture uniformity and combustion efficiency. Indeed, high-fidelity CFD models were crucial for accurately simulating hydrogen injection, combustion, and anomalies such as knock, preignition, and misfire, with the goal of achieving high efficiency and low NO_x emissions. As a result of the tradeoff between performance and complexity, the engine architecture defined for this work is based on PFI hydrogen injection. The adoption of hydrogen port injection in this work minimizes changes to the overall engine architecture, derived from a diesel engine, while future work could address the transition to DI injection and more advanced supercharging systems in order to explore further performance improvements. The simulation models have therefore been validated at the component level, also

Table 3
H_2ICE project targets for vehicle and engine efficiency, and NO_x emissions.

Vehicle performance	**Max Speed**	65 km/h
	Min Acceleration	1.1 m/s^2
	Max Gradeability @Full Load	14%
Vehicle and engine efficiency	**Specific power**	40 kW/dm^3
	ICE efficiency	42% peak efficiency 35% part load efficiency
	Fuel consumption	10 kg/100 km
Emissions	**NO_x tailpipe**	<0.05 g/kWh
Auxiliaries	**WHR system efficiency**	>4%
	eTurbo efficiency	>4%

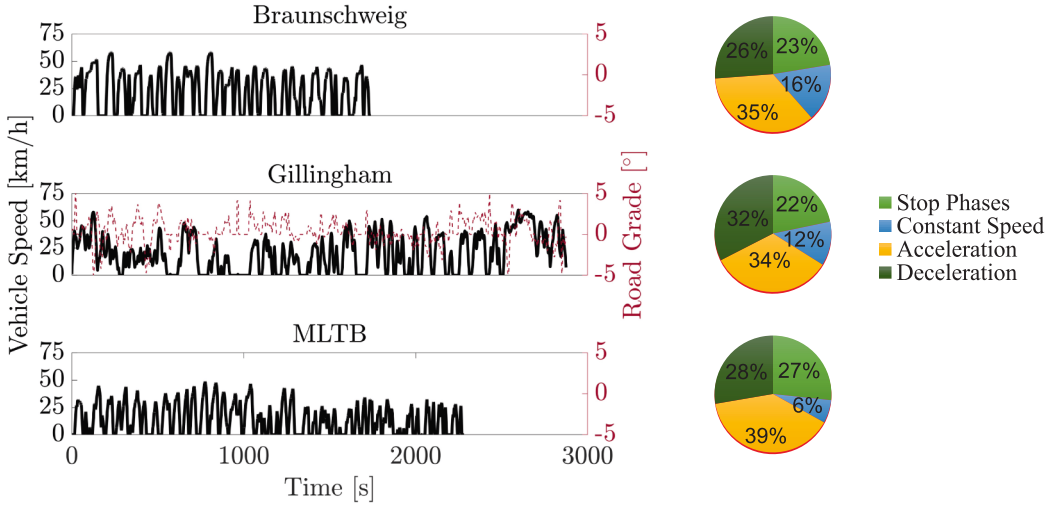

Fig. 1. Vehicle speed of the considered driving cycles (black lines), and road grade when present (red line), together with driving cycle phases. (For interpretation of the references to colour in this figure legend, the reader is referred to the web version of this article.)

taking into account future developments. This section discusses the experimental campaign in a single-cylinder research engine and the subsequent validation of a CFD numerical model for hydrogen combustion, employed to develop the engine model for the final vehicle demo.

3.1. Single-Cylinder research engine

Experiments were conducted on a 500-cc single-cylinder PFI engine with a pent-roof chamber and optical access (Fig. 2). Mixture enleanment λ was controlled at fixed airflow by regulating the hydrogen injection duration, while combustion and emissions were monitored using standard indicating equipment and a fast lambda/NOx analyzer. A high-speed camera provided combustion visualization. More details can be found in [26–29]. It is worth noting that the optical engine geometry (pent-roof) differs from the final heavy-duty bus engine; however, it serves as a fundamental platform to validate the hydrogen combustion physics and calibrate the CFD combustion and emission sub-models.

3.2. 1D and 3D-CFD models

The single-cylinder engine is modeled via a system-level tool (GT-Power) and a detailed CFD tool (CONVERGE), shown in Fig. 3, left.

The 1D engine model features the full intake and exhaust systems, with the hydrogen injection into the intake manifold after the throttle valve, and a specific model to account for blow-by through the piston rings, which is crucial for accurately interpreting the optical engine measurements. To model combustion, a two-zone predictive model is used, namely, the spark-ignition turbulent-flame (SITurb) model [30,31]. For hydrogen, it is worth mentioning that only a proprietary model for the laminar flame speed is available. A proper preliminary calibration has been performed against measured data to set the combustion model constants following the procedure reported in [32]. The calibration resulted in these values for the combustion model parameters:

- Flame Kernel Growth Multiplier = 1.5
- Turbulent Flame Speed Multiplier = 1.1
- Taylor Length Scale Multiplier = 2.2
- Overall Convection Multiplier = 1.0
- Dilution Exponent Multiplier = 1.2.

The 3D-CFD model reproduces the geometry of the actual combustion chamber and includes truncated intake and exhaust pipes, with boundary conditions provided by a combination of indicating data and 1D simulation results. In particular, boundary conditions include time-varying pressures, temperatures, and species compositions at the inlet and outlet, with hydrogen and air assumed to be perfectly mixed at the inlet. Moreover, the 3D model does not include blow-by to facilitate the stability of the solution of the conservation equations. Unsteady Reynolds Averaged Navier-Stokes (U-RANS) equations are solved with the RNG k-ε closure for turbulence. Fixed and adaptive mesh refinements are applied to better capture the flame front and the flow structures originating from the charge motion [33,34]. Specific refinements around the spark plug, with a minimum size of 0.125 mm, support the ignition stage [35]. Specific details on the CFD setup are given in [23–25]. The G-equation combustion model is used for this activity, with an ignition source of passive G in a sphere located between the spark electrodes. The laminar flame speed table, S_L, is obtained via the C3MechV3.3 reaction mechanism for hydrogen [36]. The turbulent flame speed, S_T, uses the formulation proposed by Peters [37], with the model constant b_1 set to 3.0 for all cases [38] to match the experimental burn rate, while standard values of the turbulence-model parameters were retained. Lastly, thermal NO_x emissions are calculated by adopting the extended Zeldovich mechanism [39], both in the CFD model and in the system-level model. Experimental data, based on in-cylinder pressure measurements, emissions, and flame imaging [40,41], were essential for fine-tuning the predictive combustion and emission models.

3.3. Combustion model calibration

Engine tests and corresponding simulations have been conducted at 1000 rpm, under part load from 2 bar up to 5 bar Indicated Mean Effective Pressures (IMEP), at various dilution levels from λ = 1.6 up to λ = 3.0. Ignition Timing (IT) sweeps have been conducted for each operating point under consideration to determine the Maximum Break Torque (MBT) value in each case. All results presented in the following refer to MBT timings, and are characterized by a COV (Coefficient of Variation) of IMEP below 3–5%.

Detailed 3D investigations of the combustion development have shown that the flame front shape is rather spherical, with minimal deformation under these conditions, but with some transport attributed to the residual tumble motion. Fig. 3 indeed shows an example of the comparison between of the binarized flame image obtained from the

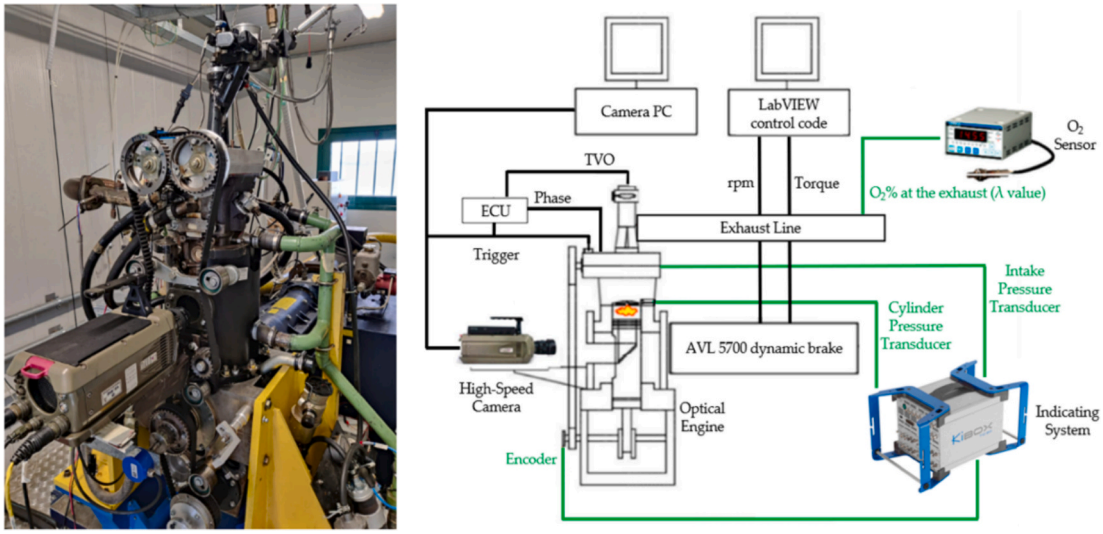

Fig. 2. Optical access engine and schematics of the data acquisition systems.

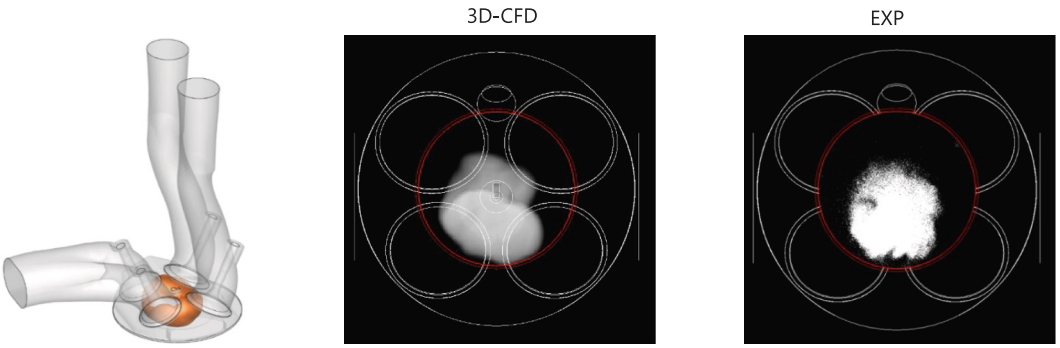

Fig. 3. Single cylinder engine modeled in Converge (left). Comparison of binarized flame image (right) and 3D-CFD volume rendering of burned gas region (middle), at 10 CAD after ignition timing (IT = −11 CAD aTDC), for the 2.5 bar IMEP case (λ = 1.6, low load). Red circles denote the quartz piston (optical limit). (For interpretation of the references to colour in this figure legend, the reader is referred to the web version of this article.)

high-speed video experiments and the corresponding CFD flame visualized through volume rendering, for the 2.5 bar IMEP case (λ = 1.6, low load). Predictions agree well in terms of shape, location, and impact with the piston.

Fig. 4 shows the in-cylinder pressure and the mass fraction burned for three dilution levels at ~ 3.5 bar IMEP, obtained from experiments and CFD simulations. The results indicate a very good agreement between both types of simulations and experiments. Pressure trends and combustion phasing are properly captured. Peak pressure and its location show minimal deviations between experimental and 1D simulated data. Similarly, the mass fraction burned curves align closely, with slight differences in the overall combustion duration mainly for the CFD models, which can be ascribed to the complex phenomena occurring at the ignition stage.

Fig. 5 reports the NO_x emission levels measured under two lambda sweeps, carried out at constant throttle, and therefore decreasing IMEP, resulting in two series at 2.2–2.5 bar and 3.5–4.5 bar. The trend shows a decrease in IMEP as lambda increases, which aligns with expectations since leaner mixtures result in lower in-cylinder combustion pressures. As expected, nitrogen oxide concentrations decrease remarkably from 1.6 to 2.3 relative air–fuel ratio, as a result of the combustion temperature drop. Simulations are in very good agreement with measurements, confirming the validity and robustness of the 1D and 3D models. As displayed in Fig. 4 and Fig. 5, a strong correlation is observed between 1D simulations, 3D-CFD results, and experimental data.

Overall, these activities focused on developing 1D and 3D-CFD models based on the UniPG single-cylinder engine data, using thermo-fluid-dynamic simulations. Ultimately, RANS simulations helped to

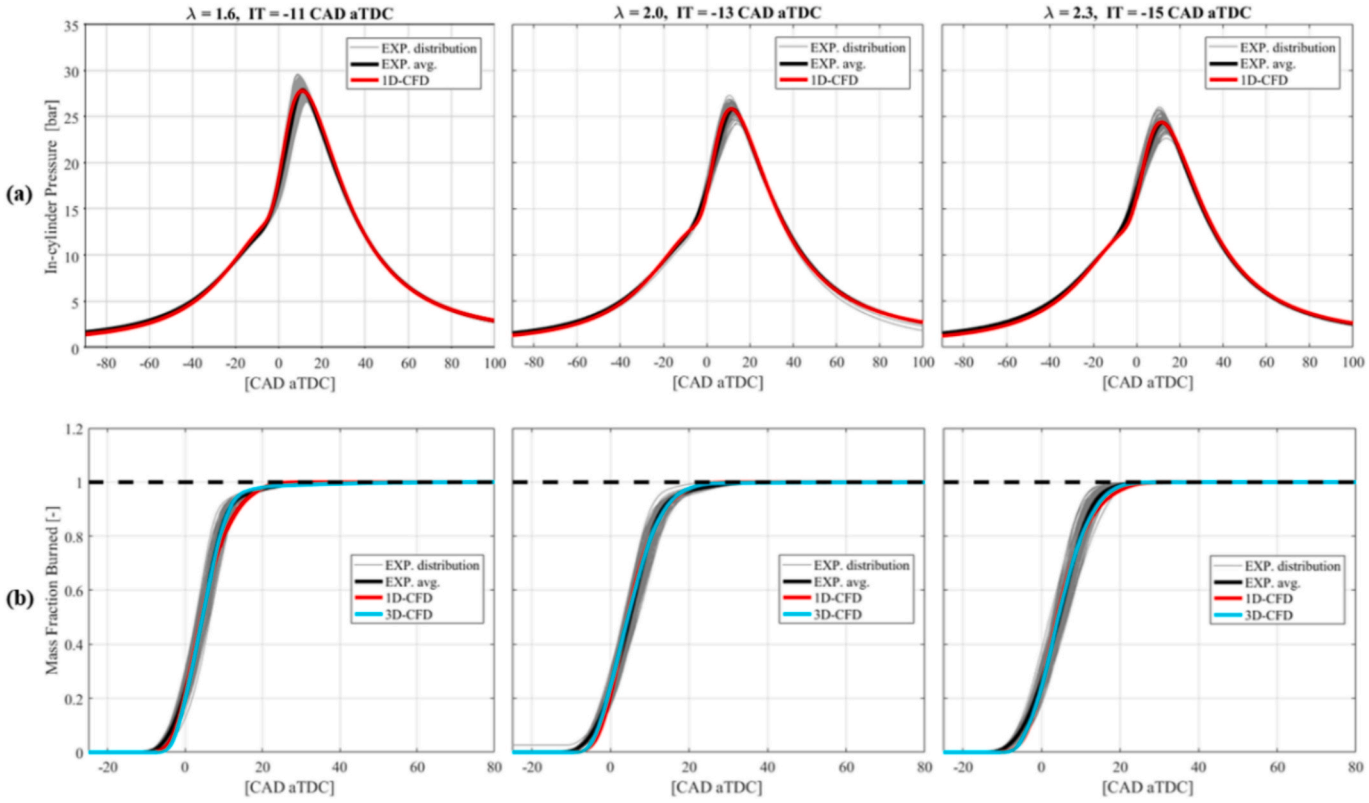

Fig. 4. Measured and simulated in-cylinder pressure (a) and the mass fraction burned (b) curves, for λ = 1.6 (left), 2.0 (middle), and 2.3 (right), at MBT ignition timing and ~ 3.5 bar IMEP.

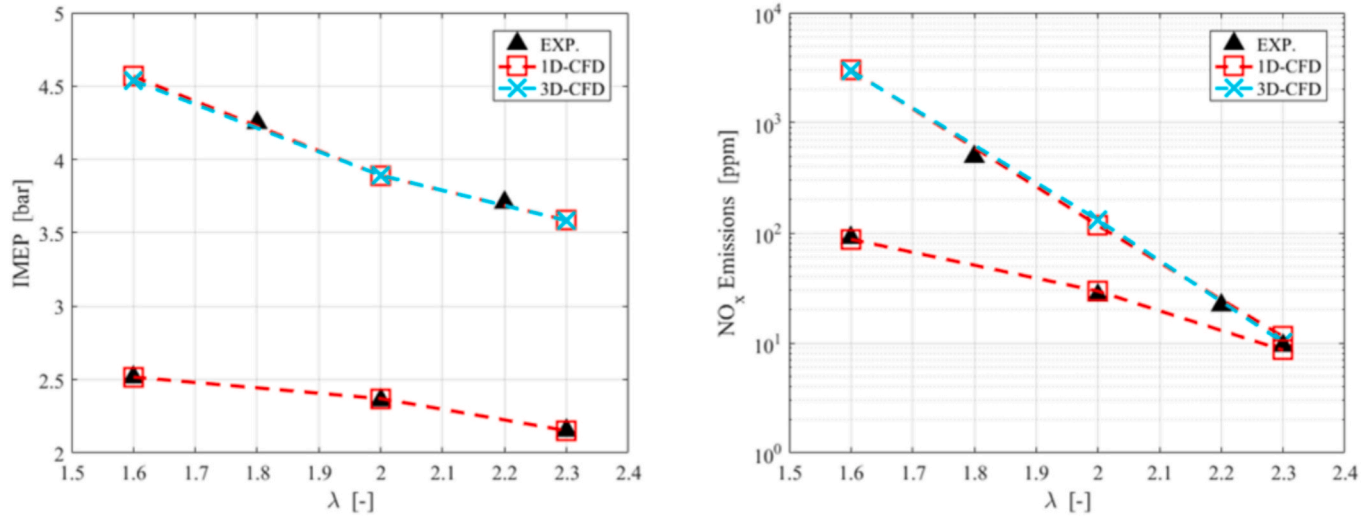

Fig. 5. Measured and simulated IMEP (left) and NOx emissions (right) for two lambda sweeps at different engine loads.

refine the injection system [17], ignition system [42] and the combustion chamber geometry of the urban bus engine to meet performance targets (efficiency peak > 42% and ultra-low NOx as reported in Table 3). Moreover, the 3D-CFD model provides heat release data and emissions, which are also integrated into the 1D model. The physical models, transferred to the urban bus engine, are then used to analyze various parameters, including ignition timing, dilution, or Exhaust Gas Recirculation (EGR) rates, and boost levels under different operating conditions across the engine operating map.

4. Waste heat recovery technologies and after treatment system

In this work, a tailored WHR section was developed and integrated into the ATS to achieve high overall system efficiency and low NO_x emissions, in line with the stated objectives. A two-stage waste heat recovery configuration was implemented (see Fig. 6). The first stage comprises an additional turbine installed in the exhaust line downstream of the turbocharging unit's main turbine, directly converting the residual gas pressure into mechanical power. The second stage employs an Organic Rankine Cycle (ORC) unit to indirectly convert exhaust heat into electrical power. The ATS section is positioned immediately downstream of the turbocharger to ensure exhaust gas temperatures remain within the optimal range for effective emission reduction across various engine operating conditions.

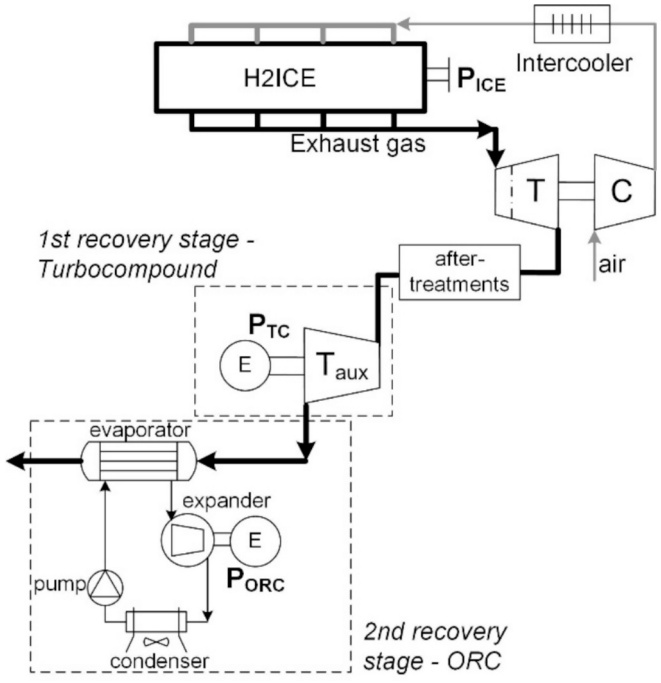

Fig. 6. Two-stage WHR recovery section considered.

4.1. Turbocompound

The first section is configured as a direct heat recovery: the exhaust gases cross a radial turbine, expanding and converting their enthalpy into mechanical power, which is subsequently transformed into electrical power via an integrated generator. This recovery turbine, referred to as the Turbocompound (TC), is of radial type, similar to that commonly used in turbocharger units. Its preliminary design was based on the similarity theory applied to the turbocharger turbine, as both operate with the same exhaust mass flow rate and comparable order of magnitude of temperatures and pressures [43]. The design point, shown in Table 4 and with a "blue circle" in Fig. 8, corresponds to an engine operating condition of 3400 rpm and 230 Nm, yielding a rated brake power of approximately 80 kW. This sizing enables the additional turbine to operate effectively even at lower engine loads, by acting on the turbine revolution speed.

This configuration was included in the overall simulation model to evaluate its interactions with the engine and potential side effects arising from the addition of a component in the exhaust line, including its influence on engine performance, turbocharger balance, and, more broadly, the adjustment of engine control parameters. Fig. 7 represents the characteristic map of the designed turbine, showing the reduced mass flow rate $\dot{m}_{red}$ [(kg/s)$K^{0.5}$/kPa], evaluated at the gas inlet pressure and temperature, as a function of the expansion ratio β. The turbine adiabatic efficiency η_{TC}, as defined in Equation (1), is also reported. Based on these data, the power recovered by the TC, P_{TC}, can be determined. Revolution speed is not reported, but it can be changed according to an optimization of the overall system [44]. This approach consented to keep the physical consistency of the analysis, and consider

Table 4
Exhaust gas thermodynamic data chosen for the design point of the turbocompound.

Pressure gas [bar]	Temperature gas [°C]	Gas flow rate [g/s]
1.35	442.4	160.2

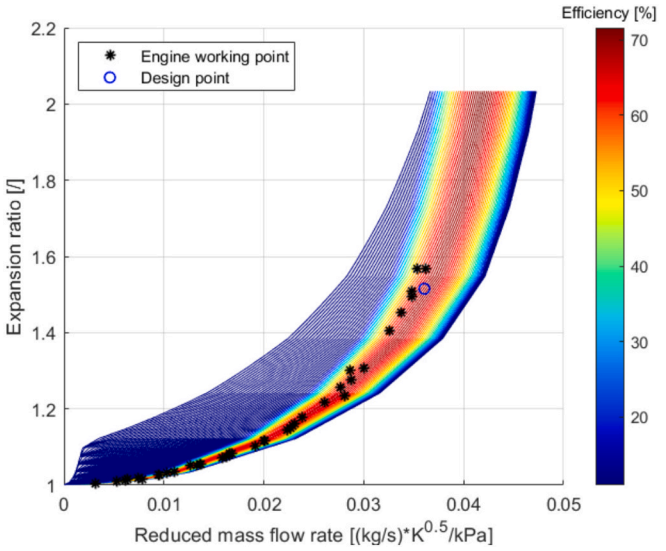

Fig. 7. Characteristic map of the additional turbine proposed for the first WHR section. The working points of the H_2ICE engine have also been plotted.

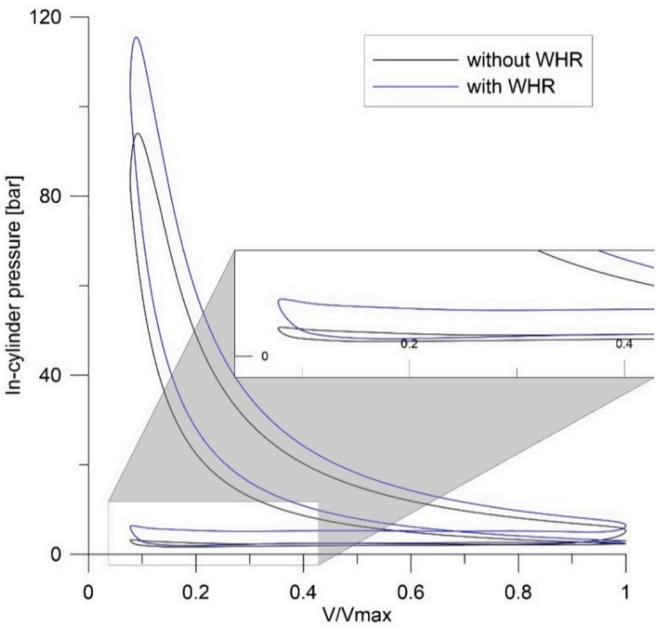

Fig. 8. Indicated cycles for a specific working point, with and without recovery sections in the exhausts.

at the same time the variation in gas composition, temperature and pressure (Equation (1).

$$\begin{cases} \dot{m}_{red} = \dfrac{\dot{m}_{gas}\sqrt{T_{in,TC}}}{p_{in,TC}} \\ \beta = \dfrac{p_{in,TC}}{p_{out,TC}} \\ P_{TC} = \eta_{em}\eta_{TC}\dot{m}_{gas}\left(h_{in,TC} - h_{out,TC,ad-is}\right) \end{cases} \quad (1)$$

In addition, the considered working points of the H2ICE engine have also been plotted. The selected turbine design point lies in the high-load region, ensuring good efficiency across most of the engine operating conditions considered (up to 50%). The maximum efficiency slightly exceeds 70%.

An electromechanical efficiency, η_m, is considered to account for the conversion of recovered thermodynamic power into electrical power. The high-speed electrical generator coupled to the TC unit has an efficiency profile obtained from literature data [45], encompassing both electrical and mechanical conversion losses. This efficiency varies parabolically with rotational speed, reaching a maximum of 92% at approximately 70 kRPM and remaining above 85% in the range of 40–100 kRPM, indicating high performance across the most frequently encountered operating conditions. An important effect to consider is the increase in the exhaust backpressure, which leads to higher pumping losses and, consequently, an increase in specific fuel consumption or a reduction in useful torque. Fig. 8 shows the indicated cycle (in-cylinder pressure vs. volume) of the H_2ICE at an engine operating point of 3400 RPM and 230 Nm (BMEP = 4.8 bar), comparing the baseline configuration (without the direct WHR) to the case with the TC operating and inducing backpressure (in-cylinder pressure variation during exhaust phase). The results highlight that while the pumping loop becomes more pronounced, its adverse impact is partially offset by the increased engine inlet pressure, which raises the pressure levels throughout the thermodynamic cycle and enhances the positive (upper) portion of the cycle. Nevertheless, the increase in peak in-cylinder pressure should be managed to avoid knocking and excessive NO_x emissions.

4.2. ORC

The ORC unit was modeled using an integrated zero-dimensional (0D) and one-dimensional (1D) approach within the GT-SUITE™ environment. The system's primary goal was to simulate the off-design performance of a small-scale ORC-based unit fed by the exhaust gases. Thermodynamic properties of the working fluid (R245fa) were retrieved using the NIST Refprop™ database.

The ORC-based unit considered consists of: a) a volumetric gear *pump*, which delivers the working fluid into the system. It was modeled using a 0D approach, where its mass flow rate was derived from the mass conservation equation; b) a scroll-type *expander*, able to convert thermal energy into mechanical form. It was modeled using a map-based approach derived from experimental data, given its crucial role in determining system behavior; c) heat exchangers (*evaporator* and *condenser*), represented as 1D discretized elements where mass, energy, and momentum conservation equations were applied. Heat transfer coefficients were evaluated using established correlations such as Colburn, Kandlikar, and Friedel ones; d) a three-liter tank serves as a receiver upstream of the pump, ensuring flow stability and pressure head on the pump. The system of Equation (2) reports the most relevant relations. The model is initialized by the inlet pressure, temperature, and mass flow rate of the exhaust gas, which serve as an input for calculating the thermal power transferred ($\dot{Q}_{rec}$) to the working fluid within the Heat Recovery Vapor Generator (HRVG). This calculation enables the evaluation of the mass flow rate of the working fluid, $\dot{m}_{WF}$, given that the inlet and outlet fluid enthalpies, $h_{evap,in}$ and $h_{evap,out}$, are defined by the pump discharge and expander inlet. Once the R245fa mass flow rate is calculated, the expander and pump thermodynamic power can be estimated, with their efficiencies taken from experimentally based operating maps. Pressure losses along the piping are also evaluated to determine the actual inlet and outlet conditions of the working fluid for each component. Final net electrical power output, P_{ORC}, is obtained by applying the electrical efficiency of the generator coupled to the turbomachinery.

$$\begin{cases} \dot{Q}_{rec} = \dot{m}_{gas} c_{p,gas} \left(T_{gas,in} - T_{gas,out}\right) \\ \dot{m_{WF}} = \dfrac{\dot{Q}_{rec}}{\left(h_{evap,out} - h_{evap,in}\right)} \\ P_{exp} = \dot{m}_{wf} \left(h_{exp,in} - h_{exp,out}\right) \eta_{exp} \\ P_{pump} = \dot{m}_{wf} \left(h_{pump,out} - h_{pump,in}\right) \eta_{pump} \\ P_{ORC} = \eta_{el,exp} P_{exp} - \dfrac{P_{pump}}{\eta_{el,pump}} \end{cases} \quad (2)$$

The model is completed with the hydraulic permeability evaluation, which correlates the evaporating pressure with the mass flow rate. Experimental results from [46] confirmed that this relationship is approximately linear, enabling the design of a proportional regulator for system control.

The overall model of the ORC-based unit was validated using experimental data collected from a test bench at the University of L'Aquila ICE lab. The validation was performed under both steady-state and dynamic conditions [47]. The model accuracy was evaluated by comparing predictions to experimental data under step variations of ICE torque and speed, with a relative error in predicting expander intake pressure equal to 2.3% before and 0.1% after step changes. The validated model was therefore considered sufficiently robust to serve as a simulation platform for evaluating ORC performance and testing control strategies.

Based on the verified linear relationship between expander inlet pressure and mass flow rate, a proportional regulator was implemented to improve performance under off-design conditions. The regulator gain was experimentally determined from test data, and the control strategy combined feedforward and feedback actions [48], allowing further optimization of unit performance. Fig. 9 presents the net electrical power output of the ORC unit as a function of the thermodynamic conditions of the exhaust gas entering the evaporator (temperature and reduced mass flow rate). The maximum recovered mechanical power reaches 2 kW at the highest exhaust temperature and mass flow rates, corresponding to an ORC efficiency of 5%, exceeding the project's target. The figure also highlights the operating range of the ORC-based unit, including the minimum temperature and flow rate thresholds required for positive energy recovery.

Fig. 10 shows the net electrical power recovered by the two-stage WHR as a function of the exhaust energy available downstream of the turbocharger, $Q_{exh,available}$, calculated according to Equation (3) with a reference temperature $T_{ref} = 298$ K. Under maximum exhaust energy conditions, the total recovered electrical power approaches 16 kW. The TC stage contributes the majority of this output, while the ORC-based unit accounts for approximately 10–12% of the total power, in accord to expectation [49,50]. The design target was to achieve a WHR efficiency above 4%, with an e-turbo efficiency of 4%. As shown in the figure, and using Equation (3) for efficiency calculation, the TC recovery efficiency, $\eta_{rec,TC}$, reaches up to 12%, with an average value of 4.2%, while the overall WHR efficiency, η_{WHR}, reaches 14% in the best case, and an average value of 6.4%, across the range of operating points considered, which span a wide portion of the engine map.

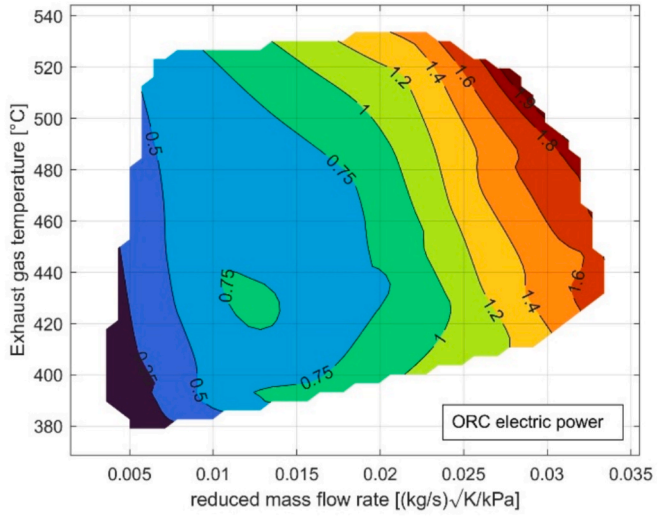

Fig. 9. Final ORC electrical power produced in relation to the exhaust gas conditions at the evaporator inlet.

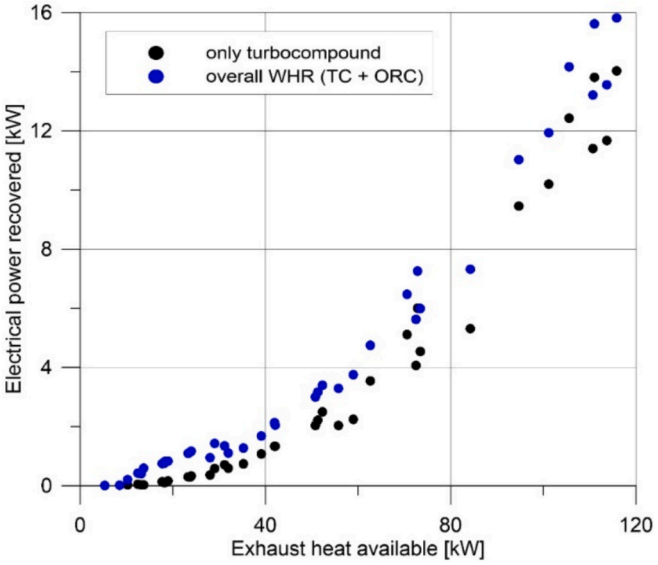

Fig. 10. Power recovered in electrical form from the two recovery sections.

$$\begin{cases} Q_{exh,available} = m_{gas} c_{p,gas} \left(T_{gas,exh} - T_{ref}\right) \\ \eta_{rec,TCo} = \dfrac{P_{el,TCo}}{Q_{exh,available}} \\ \eta_{WHR} = \dfrac{P_{el,TC} + P_{el,ORC}}{Q_{exh,available}} \end{cases} \quad (3)$$

The achieved target in terms of net recovered power and efficiencies fall within the experimental experience of both TC and ORC system, ensuring effective recovery with low cost-benefit ratio [51,52].

4.3. H_2-SCR system

Although the H2 engine is intended to operate with extreme lean mixtures, thus producing low NO_x emissions, the hybrid-bus application targets near-zero emissions. Therefore, NO_x abatement by the ATS is still mandatory. Currently, the conventional SCR system employs ammonia (NH_3-SCR) to catalytically convert NO_x into nitrogen (N_2) and water (H_2O). Due to the toxicity and hazardous nature of ammonia, it is produced in vehicles using an aqueous solution containing 32.5 wt% urea $CO(NH_2)_2$, requiring on-board storage systems for urea. Although ammonia and urea are currently the preferred choice for the SCR of NO_x, hydrogen has recently emerged as a promising alternative. Indeed, in recent years, several researchers have focused their studies on the development of a suitable catalytic system for the SCR of NO_x by using hydrogen [53,54].

H_2-SCR technology addresses several limitations associated with ammonia-based SCR, including issues related to urea decomposition, ammonia slip, byproduct deposition, and low efficiency during cold-start conditions (light-off temperature is about 200 °C). Specifically: *i*)

H_2 is readily available to participate to the reduction reaction; *ii*) no additional reductant storage tank or ammonia slip catalyst is required; *iii*) higher low-temperature activity is achieved compared to NH_3-SCR, enabling significant NO_x reduction at temperatures below 170 °C, thus being suitable for exhaust gas treatment during engine cold-start and urban-driving operations [53].

To assess the potential NO_x reduction efficiency of H_2-SCR technology in the H_2 engine, three catalytic systems were prepared and experimentally evaluated [17]: 1) Pd/CeO_2-ZrO_2; 2) Pd/CeO_2-Al_2O_3; 3) Pd/TiO_2-Al_2O_3.

For all the catalytic systems, the monolithic substrate of the sample is composed of cordierite, and the active component is palladium (Pd). The cordierite monolithic substrate was coated with the supported catalysts according to the impregnation method procedure. XRD (X-Ray diffraction) and SEM (Scanning Electron Microscopy) analyses were performed on the activated catalyst samples at the end of the impregnation procedure, to verify the proper composition of the catalytic system and the actual dispersion of the active components and support material on the monolithic substrate [17,55].

The three catalyst samples were tested on the synthetic gas bench of the Clean Mobility and Thermofluids research center of the Universitat Politècnica de València, which allows generating the desired gas mixtures by managing independently the species concentration, mass flow rate, temperature, and pressure. Different analyzers, including Fourier transform infra-red spectroscopy and gas chromatograph analyzers, are used to measure the gas concentration at the catalyst inlet/outlet.

The experimental tests on the SCR samples were designed with the aim of evaluating the NO conversion efficiency and N2-selectivity of the catalyst operating under real conditions with respect to the final application at the exhaust of an H_2ICE. Therefore, the reagent mixture composition was set according to the engine exhaust gas simulated by the 1D model described in Section 5 in the operating condition corresponding to an engine speed of 3000 rpm and λ equal to 2.0 (lean-burn condition).

The experimental tests were performed at different reaction temperatures, O_2 concentration in the reagent mixture, space velocity, H2/NO ratio, and in dry/wet gas mixture conditions (0% or 10% H2O concentration) while the inlet NO concentration was set to 350 ppm in all cases.

The Design of Experiment (DoE) is shown in Table 5 [55].

The experimental results achieved on the catalytic sample #3 (Pd/TiO2-Al2O3), which has shown the most promising features compared to the other catalytic systems (sample#1 and #2), are reported in Fig. 11. The figure shows the NO Conversion Efficiency, N_2-Selectivity and NH_3 concentration as a function of the catalyst temperature at different O_2 inlet concentrations, with a reaction ratio H_2/NO of 13 and space velocity of 30 k 1/h.

The results evidence that the NO Conversion Efficiency increases with the catalyst temperature and decreases with the oxygen concentration, by reaching 50% at the condition of H2/NO ratio equal to 13, SV equal to 30 k 1/h, system temperature of 250 °C and O2 inlet concentration equal to 12.5%, that is very close to the real expected condition at the engine exhaust.

Fig. 12 reports the results related to the catalyst operating in wet conditions, with H_2O concentration in the reagent mixture of 10%. The figure shows NO Conversion Efficiency, N_2-Selectivity, and NH_3 concentration as a function of O_2 inlet concentration for different H_2/NO reaction ratios, with a catalyst temperature of 190 °C and space velocity of 50 k 1/h.

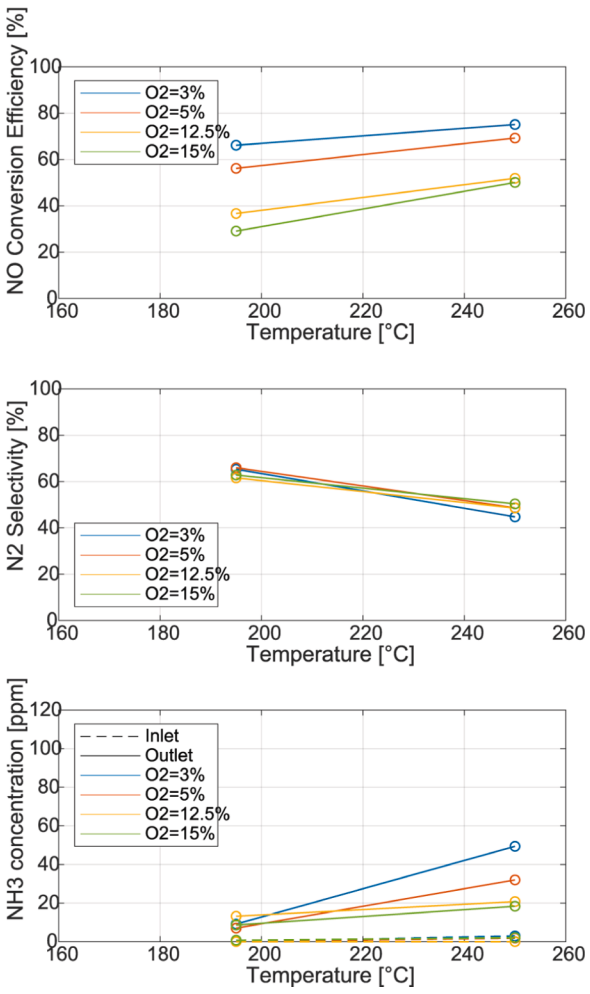

Fig. 11. Pd/TiO_2-Al_2O_3 sample NO Conversion Efficiency (top), N_2-Selectivity (middle), NH_3 Concentration (bottom) at H_2/NO ratio = 13, Space Velocity = 30 k 1/h.

The results evidence the expected performance deterioration in *wet* reaction conditions, but it is still observed that the conversion efficiency reaches almost 50%, with H_2/NO equal to 16, O_2 inlet concentration equal to 12.5% and system temperature of 190 °C, which is a very promising result. Analysis of the product distribution further clarifies the behavior of the Pd/TiO_2–Al_2O_3 catalyst under the conditions studied. As shown by the trends, NO conversion increases systematically when the H_2/NO ratio is increased from 8 to 13 and 16, in accordance with the expected improvement in reduction efficiency when an

Table 5
DoE of the experimental tests on the H_2-SCR.

T [°C]: ± 30		O2 inlet concentration			
		3%	5%	12.5%	15%
Space Velocity:	30 k 1/h	Reaction ratio (H2/NO) = 8, 13, 16	Reaction ratio (H2/NO) = 8, 13, 16	Reaction ratio (H2/NO) = 8, 13, 16	Reaction ratio (H2/NO) = 8, 13, 16
	50 k 1/h	Reaction ratio (H2/NO) = 8, 13, 16	Reaction ratio (H2/NO) = 8, 13, 16	Reaction ratio (H2/NO) = 8, 13, 16	Reaction ratio (H2/NO) = 8, 13, 16
	85 k 1/h	Reaction ratio (H2/NO) = 8, 13, 16	Reaction ratio (H2/NO) = 8, 13, 16	Reaction ratio (H2/NO) = 8, 13, 16	Reaction ratio (H2/NO) = 8, 13, 16

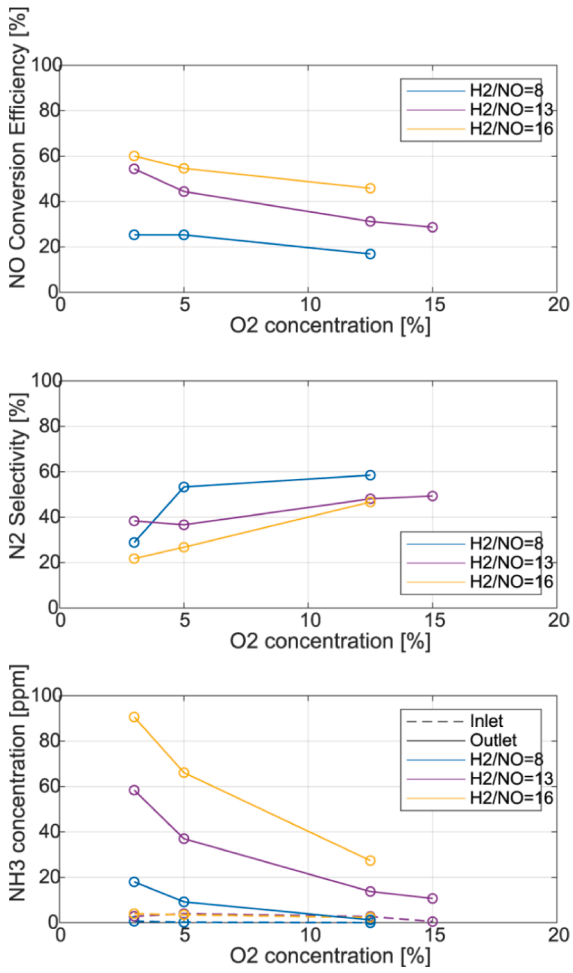

Fig. 12. Pd/TiO_2-Al_2O_3 sample NO Conversion Efficiency (top), N_2-Selectivity (middle), NH_3 Concentration (bottom) in wet condition: H2O concentration = 10%, Temperature = 190 °C, Space Velocity = 50 k 1/h.

additional reducing agent is available. At the same time, higher H_2/NO ratios lead to an increase in the concentration of NH_3 at the reactor outlet, while the selectivity of N_2 remains essentially constant under all conditions examined. This indicates that the reaction network progressively shifts from NO towards the fully reduced products (N_2 and NH_3), reducing the fraction of unconverted NO and the undesirable partially oxidized product, N_2O. It is formed under more oxidizing conditions or at elevated temperatures; therefore, increasing the O_2 concentration or operating temperature typically shifts the equilibrium towards this partially oxidized species. From an application point of view, the NH_3 formed in situ could be advantageously exploited in a downstream catalytic stage, allowing a further reduction in NOx of approximately 12%, ultimately bringing the overall removal efficiency to over 60%. This behavior is particularly relevant at low temperatures that also ensure lower catalyst deactivation [56–58], where this catalyst operates most effectively, before side reactions at higher temperatures increasingly favor the formation of N_2O. In conclusion, it is worth remarking that the Pd/ TiO_2-Al_2O_3 catalytic system has a Pd load that is half of the other systems (0.5 vs. 1 wt%) and is therefore more affordable and cost-effective.

5. Engine and hybrid powertrain management

The Engine and Hybrid Powertrain Management is aimed at evaluating/setting the most suitable operation of the whole powertrain system, in terms of energy consumption and tailpipe NO_x emissions. This task has been accomplished by taking into account the integration of the engine (including WHR and SCR) and the electric systems (battery pack and electric machines) into the vehicle propulsion system.

5.1. Engine control

Once the WHRs and SCR systems have been developed, it was necessary to implement a powertrain management strategy to identify the optimal operating points of the combined system (engine + WHR), while simultaneously ensuring that the SCR operates under optimal conditions. To achieve this in a simulation environment and effectively test a suitable control strategy, a reliable and accurate engine model was essential. This model served as the core of the simulation, enabling the evaluation of different control approaches under various operating scenarios and ensuring a proper balance between energy recovery and emission reduction.

Firstly, the 1-D reference engine model [22] has been integrated with the TC, the ORC and the SCR models [17,49,50]. Starting from this new configuration, a DoE has been conducted to map all the possible operating conditions of the system, aimed at calibrating a fast running 0-D model for Software in the Loop (SiL) purposes [59]. Table 6 summarizes the tests performed.

As visible from Table 6, the whole operating range has been investigated considering several combinations of different parameters, ensuring to generate a fully comprehensive dataset. For each combination of engine speed, load (BMEP), and λ, sweeps of CA50, EGR rate, and turbocompound speed were carried out, varying one parameter at a time. The 1D reference engine model includes dedicated controllers that regulate the injected fuel mass and intake manifold pressure, allowing the target BMEP to be reached for a given λ. In parallel, a dedicated EGR controller, acting on the EGR valve position, was implemented to achieve the desired EGR rate (EGR%) defined with respect to the intake air mass. Through coordinated actuation of the VGT rack, throttle, EGR valve, and fuel injection, both λ and EGR targets can be met consistently across the DoE. Following the same approach presented in [59] a 0-D fast-running control-oriented engine model has been developed in Matlab/Simulink. Dedicated artificial neural networks have been properly calibrated [59] by means of the Deep Learning Toolbox of Matlab to represent the main performance indexes. The accuracy of the model is reported in Table 7, considering the percentage Root Mean Squared Error (RMSE). In the 0D formulation, λ is directly computed as the air–fuel mass ratio; hence, λ errors arise solely from the air-path model, as the injected fuel mass is imposed to match the 1D reference (consistent with the model's fuel-input structure). Conversely, the EGR rate is calculated following the methodology introduced in [59], where the exhaust gas flow rate is modelled using several parameters, including λ, and the EGR valve position (taken from the reference model) is used to determine the resulting EGR fraction. As is visible, all the parameters present an RMSE below 2%, ensuring the good accuracy of the model. As reported in [59], the model also integrates zero-dimensional behavior of statistical phenomena such as cyclic dispersion and knock, which are modeled as Gaussian of CA50 (affecting all indicated quantities) and log-normal for the knock distributions,

Table 6
DoE of engine operating conditions.

Parameter	Units	Lower Limit	Upper Limit	Number of Levels
Engine Speed	[rpm]	1000	4000	4
BMEP	[bar]	2	Max @given engine speed	> 4
λ	[-]	2	2.7	4
CA50	[°aTDC]	0	30	7
EGR	[%]	0	7.5	4
TC Speed	[krpm]	0	100	5

Table 7
Accuracy of the engine model.

Parameter	TC Speed	Boost	MAP	λ	EGR	CA50	BSFC	P_{max}	T_{max}	IMEP	T_{exh}	P_{exh}	P_{TC}	NO_x
RMSE [%]	0.4	0.59	0.62	1	0.46	0.33	0.55	0.36	0.9	0.24	0.9	0.89	0.42	2

respectively. In particular for the knock, the model allows to provide, as a function of operating conditions such as engine speed, mean CA50, lambda, fuel mass, and EGR rate, the actual cycle-to-cycle knock index, modeled based on the maximum amplitude of pressure oscillation.

After the development of the engine model, a torque-based control strategy for H_2ICEs has been calibrated [59]. However, as the engine model features the TC [49], the procedure for the identification of the optimal operating conditions (in terms of CA50 and λ) for each combination of engine speed and load (i.e., BMEP) has to be revised to properly take into account the contribution of the TC. For this reason, a corrected Brake Thermal Efficiency (BTE*), defined in Equation (4), has been introduced in consistency with [44], where P_{ICE} represents the power produced by the engine, P_{TC} the power extracted from the TC, $\dot{m}_{H2}$ the hydrogen mass flow rate and *LHV* the lower heating value of the fuel:

$$BTE^{*} = \frac{P_{ICE} + P_{TCo}}{\dot{m}_{H2} \bullet LHV}. \tag{4}$$

In particular, for each combination of engine speed and load, BTE* has been calculated under different TC speeds, CA50 positions and dilution conditions, allowing the identification of the best operating set of parameters (after the removal of unreliable conditions).

Fig. 13 presents the comparison between BTE (a) and BTE* (c) for a fixed operating condition (λ = 2.3, 3000 rpm, 10 bar of BMEP). As visible, when combustion is retarded (starting from the CA50 that maximizes BTE), P_{TC} increases for a given TC speed (Fig. 13b) thanks to the higher energy content in the exhaust gases. However, this effect is detrimental for the combustion process, resulting in a lower conversion efficiency of hydrogen into usable work from the engine. Although P_{TC} increases, BTE* is also influenced by the hydrogen mass flow, which rises under these conditions. In fact, since all simulations are performed at fixed BMEP and engine speed, shifting the CA50 position necessarily alters the hydrogen consumption required to deliver the same BMEP. However, the electrical power recovered by the WHR system increases the total generated power (engine electrical output plus WHR recovery). Consequently, even though the hydrogen consumption is fixed for a given CA50 and turbocompound speed (as shown in Fig. 13a), the specific fuel consumption, and therefore the corrected brake thermal efficiency (BTE*), changes. This makes it possible to identify the overall optimal operating point as the condition that maximizes BTE*. Therefore, the CA50 that maximizes BTE* could not necessarily coincide with that which maximizes P_{TC}. The optimal working point (in terms of BTE*) is achieved slightly retarding CA50 relative to the baseline condition (i.e., maximum BTE). It is important to note that the working-point optimization was carried out without accounting for its impact on NOx formation but only BTE*. As a result, the optimized operating

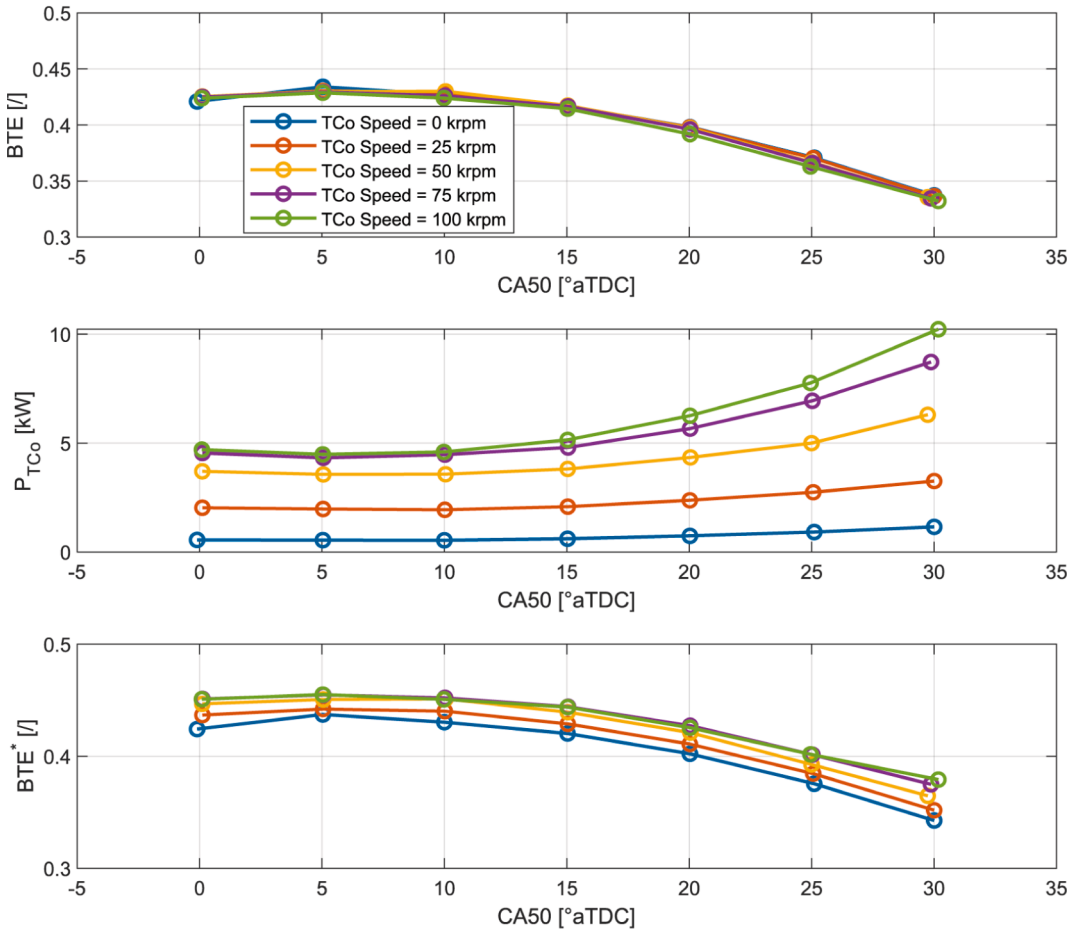

Fig. 13. BTE (top), PTC (middle) and BTE* (bottom) for fixed engine speed, λ and different TC speeds.

parameters for a given engine speed and load may produce either slightly more or less NOx than the baseline (configuration without WHRs), due to changes in the CA50 timing, λ value and EGR concentration. As a matter of fact, advancing the combustion phasing, as running the engine in less lean conditions, results in higher peak temperature, thus NOx production. Once the optimal control parameters were determined for each engine speed and load, a dedicated torque-based control strategy was calibrated [59] to ensure accurate delivery of the requested torque at a given engine speed, as already demonstrated in SiL validations [59,60]. To further enhance engine reliability, dedicated strategies have been incorporated to control knocking behaviour and limit in-cylinder maximum pressure, integrating a CA50 physics-based peak pressure model with a dedicated feedback controller [61,62]. Since these controllers rely on feedback metrics such as P_{max} and the knock index, one practical solution is to use low-cost pressure transducers [63].

The proposed control strategy is suitable for integration in existing engine control frameworks: the EMS regulates the required torque through appropriate management of H_2ICE actuators, while the target speed is maintained by the electric machine coupled to the engine.

5.2. Hybrid powertrain management

The EMS of the powertrain is aimed at controlling the power provided by the series hybrid architecture composed by the coupling of the ICE and the Electric Generator (i.e., ICE + EG) to guarantee the battery charge sustaining with the minimum energy consumption. A model of the Hybrid Electric Vehicle (HEV) has been developed to implement the EMS and assess the energy consumption for different driving cycles [17]. The final series architecture consists then in adding the TC and ORC to the exhaust of the ICE. The results of the 1D simulation analysis carried out on engine and WHR systems were considered to develop black-box models to be implemented in the HEV model (Fig. 14).

The optimal series powertrain system power profile as a function of engine speed and torque has been identified through an optimization procedure that maximizes the series system efficiency, defined as in Eq. (5):

$$\eta_{system} = \frac{P_{DC}}{P_{Fuel}} = \frac{P_{IceGen} + P_{TcGen} + P_{OrcGen}}{P_{Fuel}} \quad (5)$$

The development of the Energy Management System focused on a heuristic, causal Rule–Based (RB) strategy designed for real-time implementation on a production Engine Control Unit (ECU). For comparison purposes, a local optimization approach based on the Pontryagin Minimum Principle (PMP) was also formulated. The latter was employed to estimate a benchmark for the vehicle's fuel consumption over the entire driving cycle. In fact, the Pontryagin Minimum Principle is an optimal control framework that provides the necessary conditions for optimality, but it requires full knowledge of the driving cycle, thus leading to a non-causal solution. To assess the impact of the EMS on NO_x tailpipe emissions, the model of the ATS was integrated into the forward HEV model. This step was particularly important, as NO_x are the only relevant pollutant emissions for H_2ICEs. Moreover, series-HEVs may operate with long engine stops, which reduce exhaust temperature and in turn SCR conversion efficiency. The ATS model accounts for both the exhaust thermal dynamics and the conversion efficiency of the SCR by using dedicated sub-models. For the final integration, despite the demonstrated promising performance of the H_2-SCR, the conventional NH_3-SCR was considered instead. This option is explained considering that the NH_3-SCR is a ready-to-market technology and guarantees conversion efficiency higher than 90% in almost the whole engine operating domain of the current simulation scenario. On the other side, although the H_2-SCR exhibits significant simplification of the after-treatment layout, with benefits on capital/operation costs, and improved performance at lower exhaust temperature (e.g. during engine warm-up), at the current development stage, it still presents lower conversion efficiency when the engine operates at medium–high load. Actually, the maximum expected efficiency of 50% that can be reached considering the exhaust thermal conditions and chemical composition of the engine in the current simulation scenario, could be not sufficient to reach the project target to contain tailpipe NOx below 0.05 g/kWh, in some of the driving cycles considered.

The thermal behavior of the ATS system, adopted for the hybrid-electric bus, is simulated by an energy balance on a control volume including the SCR. The thermal model is based on the following hypotheses:

- Zero-dimensional approach;
- Lumped parameters.

According to these assumptions, the spatial variations of the temperature can be neglected, and the physical phenomena involved can only be described as a function of time, as in Equation (6):

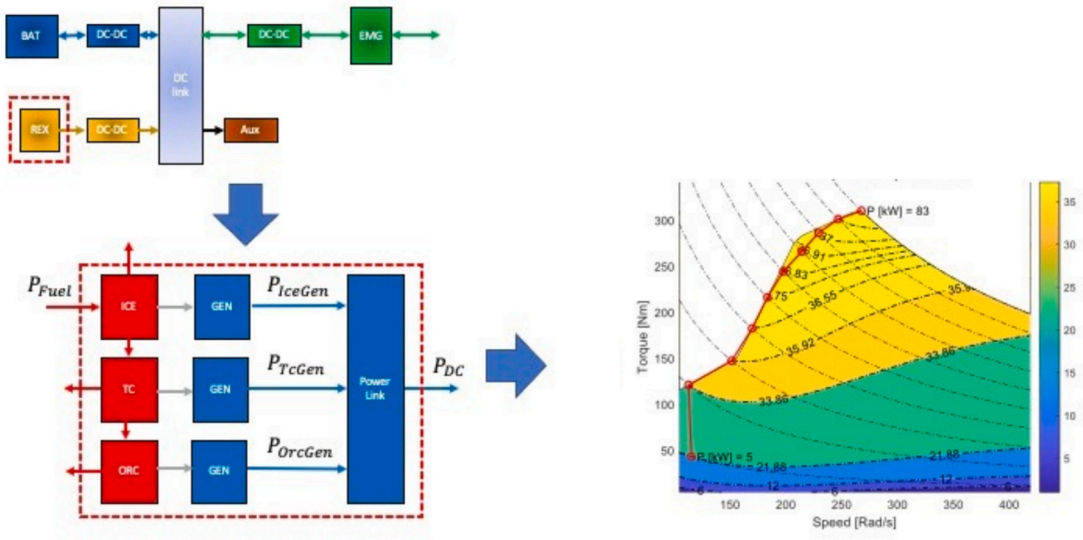

Fig. 14. HEV architecture (left) and optimal series hybrid system power profile (right).

$$\frac{\partial T_{SCR}}{\partial t} = \frac{c_{p,exh}}{C_{SCR}} * \dot{m}_{exh}(T_{exh} - T_{SCR}) - \frac{h_{amb}}{C_{SCR}}(T_{SCR} - T_{amb}) \quad (6)$$

where T_{exh} [K] and $\dot{m}_{exh}$ [kg/s] are the engine-out temperature and mass flow rate of the exhaust gases, T_{SCR} [K] is the temperature of the SCR system, that is assumed equal to the SCR outlet temperature, T_{amb}[K] is the ambient temperature, $c_{p,exh}$ [J/kg K] is the specific heat of the exhaust gases, C_{SCR} [J/K] is the SCR thermal capacity, and h_{amb} [W/K] is the convective heat transfer coefficient from the SCR to the environment.

The SCR parameters were derived from experimental data collected at the engine test bench on a different engine, subsequently scaled to match the volume of the SCR system under study. The SCR temperature estimated by the thermal model has been imposed as input to evaluate the SCR conversion efficiency, which is defined in Equation (7):

$$\eta_{SCR} = \frac{NO_{x,in}^{SCR} - NO_{x,out}^{SCR}}{NO_{x,in}^{SCR}} \quad (7)$$

where $NO_{x,in}^{SCR}$ and $NO_{x,out}^{SCR}$ are NO_x concentrations in ppm at the inlet and outlet of the SCR, respectively. The SCR conversion efficiency is determined by a black-box model, as a function of the SCR temperature [K], the Space Velocity (SV) [h^{-1}], which quantifies the velocity of the exhaust gases within the SCR, and the pre-SCR NO_2/NO_x concentration ratio. The latter has been fixed at 0.5.

5.3. Rule-Based energy management strategy

The RB strategy provides a charge-sustaining operating mode of the series system. Particularly, this mode requires that the series system is always on and operates over the whole driving cycle at constant power, specifically set for each driving cycle in order to guarantee maximum system efficiency, as well as battery charge sustaining. The workflow to evaluate the series system power set-point is shown in Fig. 15. Firstly, the road load energy demand to the DC-Link is computed by featuring a backward approach and the corresponding series system power is calculated considering the duration of the reference driving cycle. Afterwards, a simulation loop is performed by the forward HEV model to refine the power set-point that effectively guarantees the battery charge sustaining (e.g. until $|\Delta_{SOCEnd}|<2\%$).

The main results of the RB strategy are listed in Table 8, which reports a comparison of fuel consumption with and without the WHR systems.

As it can be observed, the integration of TC and ORC at ICE exhaust leads to a reduction in fuel consumption for all the driving cycles investigated, compared to the ICE-only configuration. The best result is achieved for the MLTB driving cycle. These results represent the WHR

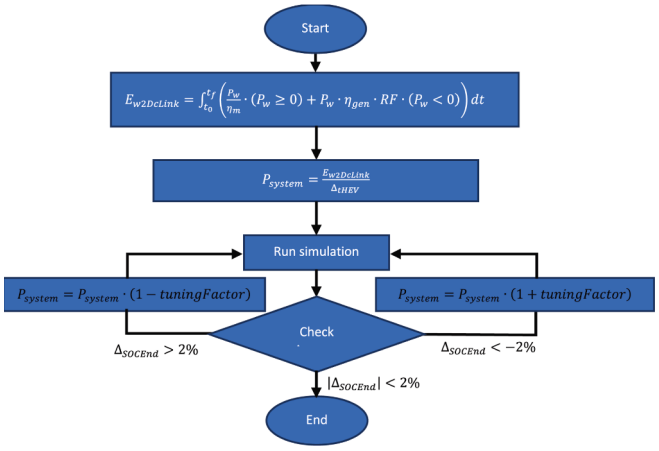

Fig. 15. Workflow of series system power set-point calculation.

Table 8
Results of the RB control strategy.

	Braunschweig		Gillingham Uphill		MLTB	
System obj. power [kW]	35.5		38.0		28.0	
	Fuel Consumption [kg/100 km] / Offset [%]					
ICE only	13.4		15.4		16.9	
ICE + TC + ORC	13.1	−2.7	15.0	−2.3	16.1	−4.5

impact at the real vehicle level, where the engine operates also at low and medium loads and the available exhaust enthalpy is limited. This explains why the fuel-economy benefit shown in Fig. 8 (ranging from 2.3% to 4.5%) is lower than the average WHR recovery efficiency quantified over the full engine operating map, where higher loads and temperatures lead to more favorable energy-recovery conditions.

5.4. Pontryagin minimum Principle

The PMP method is widely adopted for the optimal control problems of dynamic systems [64]. It aims at finding the best trajectory of the control variable that minimizes a given performance criterion, subject to the system's dynamics and constraints. The PMP problem is formulated by the system of Eqs. (8)–(11):

$$\frac{\partial \xi}{\partial t}(\xi, P_b, t) = -\frac{V_{oc}(\xi) - \sqrt{V_{oc}^2(\xi) - 4 \bullet P_b(t) \bullet R_i(\xi)}}{2 \bullet Q_{nom} \bullet R_i(\xi)} \quad (8)$$

$$\frac{\partial [\mathrm{GSLL}]}{\partial t}(\xi, P_b, [\mathrm{GSLL}], t) = -[\mathrm{GSLL}](t) \bullet \frac{\partial}{\partial \xi}\left(\frac{\partial \xi}{\partial t}\right) \quad (9)$$

$$\xi(t_0) = \xi_0 \quad (10)$$

$$\lambda(t_0) = \lambda_0 \quad (11)$$

where the Hamiltonian can be expressed as in the Equations (12) and (13):

$$H(\xi, P_b, t) = \dot{m_f}(P_b) + \lambda(t) \bullet \dot{\xi}(\xi, P_b, t) \quad (12)$$

$$P_{bOpt}(t) = argmin\{H(t, \xi, u, \lambda(t))\} \quad (13)$$

which is subjected to the constraints as in the Equations (14) – (17):

$$P_{bMaxChg}(\xi) \leq P_b \leq P_{bMaxDis}(\xi) \quad (14)$$

$$\xi_{Min} \leq \xi \leq \xi_{Max} \quad (15)$$

$$P_{system,Min} \leq P_{system} \leq P_{system,Max} \quad (16)$$

$$\left|\dot{P}_{system}\right| \leq P_{systemRateMax} \quad (17)$$

Actually, the problem is formulated by considering the battery State of Charge (SoC) as a state variable and the battery power (P_b) as a control variable. The Hamiltonian can be defined as the sum of the fuel mass consumed by the ICE and an equivalent fuel mass consumed by the electric motor, weighted by an equivalence factor, represented by the co-state. The latter drives the solution alternatively towards battery charging or battery depleting. The PMP approach minimizes the Hamiltonian while dynamically adjusting the equivalent fuel consumption factor over time, to guarantee the charge sustaining over the whole driving cycle [65]. Further improvement of the optimized EMS can be achieved by integrating a predictive model with a Spatiotemporal Attention Graph Convolutional Network (STAGCN), to forecast the passengers getting-on/off the bus and consequently the vehicle mass [66].

The results in terms of fuel consumption achieved with the RB control strategy are compared to the ones of the PMP for the three driving cycles are listed in Table 9, considering the engine configuration with and without WHR systems.

As mentioned, the PMP results represent a non-causal lower bound for fuel consumption over the driving cycle and are used as a benchmark. The comparison indicates that the RB strategy remains within approximately 5–7% of this optimum, demonstrating that the proposed implementable control achieves near-optimal performance while preserving real-time applicability. Nevertheless, even when accounting for the contribution of the WHR systems, the project target of 10 kg/100 km is not fully achieved under the current configuration. Finally, the optimal series system power trajectories have been given as input to the forward HEV model, with the SCR sub-model included, to investigate the impact of the series system control strategy on NO_x tailpipe emissions. Table 10 reports a comparison of NO_x emissions and SCR conversion efficiency between the two control strategies investigated.

The results obtained with the RB strategy highlight its capability to balance fuel consumption and NO_x emissions under realistic operating constraints. Across the investigated driving cycles, the RB control ensures limited engine-out NO_x levels, capable of meeting the project target, while maintaining competitive fuel efficiency, confirming the effectiveness of the developed causal and implementable control approach.

When compared with the RB results, the PMP-based formulation leads to higher engine-out NO_x emissions for the Braunschweig and Gillingham cycles. This increase is likely associated with the operating conditions selected by the PMP optimization, which tends to run the engine at higher load levels to minimize equivalent fuel consumption. The resulting rise in peak in-cylinder temperatures promotes NO_x formation. This behavior is consistent with the definition of the PMP Hamiltonian (Eq. (12), which focuses exclusively on fuel minimization without explicitly accounting for NO_x emissions.

6. Final virtual assessment

Once the optimal powertrain configuration was finalized, the study focused on assessing the achievement of the targets outlined in Section 2. To this end, a comprehensive digital twin was developed in the Simulink environment [67] integrating the modules of the powertrain subsystems (i.e., ICE, WHR, ATS) designed in previous tasks of the project. The analysis was conducted using the RB EMS, which was selected because it is fully causal, directly implementable on a real ECU and provides a robust trade-off between hydrogen consumption and tailpipe NO_x emissions under varying operating conditions. Vehicle simulations were performed under charge-sustaining operation, with the battery SOC maintained within a narrow band, and driver behavior was represented through PID (Proportional Integral Derivative) tracking of the prescribed cycles.

Ambient conditions were kept at standard values, and quasi-steady thermal behavior of the engine, WHR and aftertreatment systems was assumed. This modeling assumption implies that warm-up penalties, transient combustion inefficiencies, and reduced aftertreatment conversion efficiency during cold-start are not fully captured. However, in a series-hybrid urban bus application the engine typically operates within relatively stable load regions once thermal equilibrium is reached, and cold-start phases represent a limited portion of the overall duty cycle. For the considered application, the influence of thermal transients on average hydrogen consumption is therefore expected to be quite marginal.

Environmental variability related to ambient temperature was not directly parameterized in the present virtual simulations. However, climate-related effects were previously analyzed in a dedicated LCA study conducted on the same vehicle platform [12], where diverse weather conditions were explicitly considered. That analysis showed that hydrogen-consumption variations remain moderate under typical European climates and become significant only under extreme thermal scenarios. Conversely, altitude operation in terms of reduced air density and its potential impact on turbocharger performance was not explicitly modeled. The present study therefore reflects operation at standard atmospheric conditions.

The final assessment was carried out using driving scenarios not included in the powertrain design process. In particular, the SORT driving cycles have been considered [68], as standardized driving profiles specifically designed to assess the energy consumption and emissions of urban and suburban buses. The main characteristics of the mentioned driving cycles are listed in Table 11.

The SORT 1 cycle represents heavily congested urban traffic conditions, with frequent stop-and-go situations and a low average speed (≈ 12 km/h). The SORT 2 cycle is a mixed urban cycle, with a moderately higher average speed (≈ 18 km/h), less frequent stops, and a greater distance covered. Then, SORT1 and SORT2 driving cycles were considered representative of the regulatory framework. SORT3 was excluded, as it is expected to mimic suburban driving conditions, which are slightly outside the scope of the proposed vehicle concept.

In addition, an urban route measured in the Italian city of Genoa, Route 18, represents the real-world scenario for the analysis [69]. This route is characterized by significant road-grade variations and

Table 10
Comparison of NO_x emissions and SCR conversion efficiency between the two control strategies investigated, for all the driving cycles.

	Braunschweig		Gillingham Uphill		MLTB	
	Powertrain: ICE + TC + ORC					
	RB	PMP	RB	PMP	RB	PMP
NO_x Engine [mg/km]	1469	1920	1802	1956	3055	2886
NO_x Tailpipe [mg/km]	30.70	89.72	39.41	89.97	48.51	108.6
NO_x Tailpipe [g/kWh]	0.019	0.060	0.021	0.053	0.025	0.059

Table 11
Main Features of SORT driving cycles.

	SORT 1 (Heavy City)	SORT 2 (Mixed Urban)	SORT 3 (Suburban)
Avg. speed	12.6 km/h	18.6 km/h	26.3 km/h
Max. speed	40 km/h	50 km/h	60 km/h
Max. acceleration	1.03 m/s^2	1.03 m/s^2	0.77 m/s^2
Deceleration	0.8 m/s^2	0.8 m/s^2	0.8 m/s^2
Duration	154.5 s	183.9 s	206.2 s
Distance	520 *m*	920 *m*	1450 *m*

Table 9
Comparison between the results of RB and PMP control strategies for two different powertrain configurations.

	Braunschweig			Gillingham Uphill			MLTB		
	FC [kg/100 km] / Offset [%]								
	RB	PMP	Δ	RB	PMP	Δ	RB	PMP	Δ
ICE only	13.4	12.5	−7.2	15.4	14.3	−6.8	16.9	15.6	−7.4
ICE + TC + ORC	13.1	12.2	−6.5	15.0	13.8	−7.7	16.1	15.2	−5.7

congested urban traffic, providing a demanding operating profile beyond standardized cycles. The main outcomes of the simulations are reported in Table 12.

First and foremost, the analysis of these results demonstrated the robustness of the proposed EMS, as it ensures charge sustainability across a wide range of driving conditions, maintaining a negligible variation in the battery SOC. Regarding fuel economy, the results for both SORT cycles confirm that the vehicle is capable of meeting the project targets (i.e., 10 kg/100 km) in a type-approval scenario. In contrast, under the Genoa route 18, hydrogen consumption increases to 18.1–20.8 kg/100 km, approximately doubling the SORT values. This reflects the combined effect of traffic variability and topographical load changes typical of real-world operation. For context, real-world data from the Genoa transit agency indicate an average fuel consumption of approximately 1.5 km/L (on an energy equivalent basis: 2375 MJ/100 km) for conventional 12-m diesel buses on the same route [10]. When expressed on an energy-equivalent basis, the hydrogen consumption measured for the H_2ICE hybrid bus (i.e., 2280–2640 MJ/100 km) is therefore of comparable magnitude, with the forward direction slightly below and the backward direction slightly above the diesel reference. By contrast, a BEV would generally exhibit markedly lower energy consumption, although its well-to-wheel performance ultimately depends on the carbon intensity of the electricity mix [13]. Regarding NO_x emissions, under the SORT cycles NOx remain higher than the internal project target (see Section 2, target NOx emissions < 0.05 g/kWh). This behavior is mainly attributed to the frequent engine stop–start events and low-load operation typical of these short urban cycles, which limit exhaust temperature stabilization and reduce the time-averaged aftertreatment conversion efficiency. Dedicated catalyst warm-up strategies could be implemented to mitigate this aspect. Nevertheless, the obtained NO_x levels under SORT conditions (0.143–0.146 g/kWh) remain below the upcoming Euro 7 limits for HD applications (≈0.2 g/kWh), confirming compliance with the expected regulatory framework [69]. Under real-world operation on the Genoa route 18, NO_x emissions decrease to approximately 0.008–0.009 g/kWh, thereby meeting the project target (<0.05 g/kWh).

Overall, the SORT results represent reference performance under controlled operating conditions, whereas the Genoa route 18 provides a more representative estimate of consumption under demanding real-world scenarios. Variability in ambient temperature, transient thermal states, driver aggressiveness or traffic dynamics could lead to deviations from the cycle-based estimates. Quantifying such effects is a relevant direction for future work.

7. Conclusions

The H_2ICE project was conceived with the primary objective of demonstrating the technical feasibility, operational performance, and integration potential of a hydrogen-fueled internal combustion engine within a hybrid powertrain for 12-meter urban buses. The project target was to develop a CO_2 tailpipe free powertrain architecture capable of achieving a hydrogen consumption below 10 kg/100 km, and tailpipe NO_x emissions under 0.05 g/kWh, while ensuring the auxiliary systems, such as Waste Heat Recovery (WHR) and Turbo-Compound units, could provide meaningful contributions to the overall efficiency without compromising emissions.

From the combustion standpoint, advanced 1D and 3D-CFD models were developed and validated through extensive optical-engine testing, enabling the definition of stable ultra-lean operating conditions using a Port Fuel Injection (PFI) configuration selected for its reduced hardware complexity. The validated models enable optimization of ignition timing, dilution levels, and CA50 phasing.

A two-stage WHR system combining electric TC and an Organic Rankine Cycle delivered up to 16 kW of net power, with peak and average recovery efficiencies of 14% and 6.4%, respectively, confirming WHR as a viable contributor to system-level efficiency. When transferred to vehicle operation, the WHR contribution was also evaluated through the HEV model by comparing configurations with and without recovery systems. The resulting fuel-economy benefit lies between 2.3% and 4.5% depending on the mission profile, which reflects the realistic exhaust-enthalpy conditions encountered during hybrid bus operation.

Although the H_2-SCR concept demonstrated the capability to achieve up to 50% NO conversion at typical exhaust temperatures (~250 °C), confirming the technical feasibility of hydrogen-assisted NO_x reduction even with reduced palladium loading, the final virtual assessment was carried out using a conventional urea-SCR system. This choice reflects the current market maturity and technology readiness level of conventional urea-SCR, ensuring realistic and deployable emissions performance within the present regulatory framework.

Control system development was another major achievement. A torque-based engine controller was developed and calibrated for optimal Brake Thermal Efficiency (BTE) when accounting for TC contribution. Then, a causal Rule-Based (RB) Energy Management System was designed as an implementable solution for real-time ECU application. The integration of the WHR systems further contributed to improving vehicle-level fuel economy under the RB strategy, reinforcing the effectiveness of the proposed hybrid powertrain architecture.

The final virtual vehicle assessment, carried out using a quasi-static model of the complete hybrid bus, demonstrated that under regulatory SORT driving cycles the vehicle achieved hydrogen consumption as low as 9 kg/100 km and tailpipe NO_x emissions around 0.14 g/kWh, while under real-world operation NO_x emissions decreased to approximately 0.009 g/kWh. Although the internal project target for NO_x (<0.05 g/kWh) was not met under short type-approval cycles due to frequent engine stop–start events, the obtained values remain below the forthcoming Euro 7 limits for heavy-duty applications. A comparison with conventional diesel operation on the real-world conditions shows that the H_2ICE hybrid bus achieves a comparable energy consumption while delivering zero tailpipe CO_2 and reduced NO_x emissions.

Overall, the project confirms that optimized ultra-lean combustion, WHR integration, and efficient aftertreatment can enable a hydrogen-ICE hybrid bus architecture with competitive efficiency, low emissions, and operational flexibility, offering a viable decarbonization pathway where full battery-electric deployment is challenged by infrastructure or range constraints.

Future work should focus on transitioning from PFI to Direct Injection (DI) to further improve mixture control, efficiency, and lean-limit operation, as well as refining the EMS to better exploit transient operation. The integration of cost-optimized H_2-SCR technology remains a promising avenue for lowering NO_x emissions without urea logistics. In addition, dedicated catalyst warm-up strategies could be implemented to mitigate NOx emission rise in engine stop-start events. Additional work should also address cost competitiveness, durability of hydrogen-combustion hardware, and system-level safety considerations, which are essential for large-scale deployment.

Table 12
Comparison between the results with RB control strategy for the final vehicle model on SORT and RDE driving cycles.

	SORT1	SORT2	Route 18 — Forw.	Route 18 — Back.
Δ_{SOC}	−0.032	−0.031	−0.02	−0.003
FC [kg/100 km]	9	9.2	18.1	20.8
NOx Emissions [mg/km]	154	157	19	19
NOx Emissions [g/kWh]	0.146	0.143	0.009	0.008

CRediT authorship contribution statement

B. Peiretti Paradisi: Writing – review & editing, Writing – original draft, Validation, Methodology, Investigation, Data curation. **F. Millo:**

Supervision, Resources, Project administration, Methodology, Funding acquisition, Conceptualization. **L. Rolando:** Writing – original draft, Validation, Methodology, Investigation, Formal analysis, Data curation. **D. Di Battista:** Writing – review & editing, Supervision, Resources, Project administration, Funding acquisition, Conceptualization. **F. Di Prospero:** Writing – original draft, Visualization, Validation, Investigation, Formal analysis, Data curation. **E. Corti:** Writing – review & editing, Supervision, Resources, Project administration, Methodology, Conceptualization. **P.P. Brancaleoni:** Writing – original draft, Validation, Methodology, Investigation, Formal analysis, Data curation. **M. Battistoni:** Writing – review & editing, Resources, Project administration, Methodology, Funding acquisition, Conceptualization. **J. Zembi:** Writing – original draft, Visualization, Validation, Methodology, Investigation, Formal analysis. **I. Arsie:** Writing – review & editing, Supervision, Resources, Project administration, Methodology, Conceptualization. **A. Occhicone:** Writing – original draft, Visualization, Validation, Software, Formal analysis, Data curation. **M.R. Crispi:** Writing – original draft, Visualization, Validation, Methodology, Investigation, Data curation.

Funding

Research funded by Ministero dell'Università e della Ricerca (MUR). Grant number: 2020R92Y3Z.

Declaration of competing interest

The authors declare that they have no known competing financial interests or personal relationships that could have appeared to influence the work reported in this paper.

Acknowledgements

The authors would like to express their sincere gratitude to Professor Roberto Cipollone from Università dell'Aquila for his invaluable supervision, guidance, and insightful feedback throughout the course of this project.

Data availability

Data will be made available on request.

References

[1] UITP, An overview of clean buses in Europe Clean Bus Report, https://cms.uitp.org/wp/wp-content/uploads/2022/05/ASSURED-Clean-Bus-report_final2.pdf, Jan. 2024.
[2] Acar C, Dincer I. The potential role of hydrogen as a sustainable transportation fuel to combat global warming. Int J Hydrogen Energy 2020;45(5):3396–406. https://doi.org/10.1016/j.ijhydene.2018.10.149.
[3] Heid, B., Martens, C., and Orthofer, A., How hydrogen combustion engines can contribute to zero emissions, https://www.mckinsey.com/industries/automotive-and-assembly/our-insights/how-hydrogen-combustion-engines-can-contribute-to-zero-emissions, 2021.
[4] Luo QHe, Hu JB, Sun BG, Liu FS, Wang X, Li C, Bao LZ. Experimental investigation of combustion characteristics and NOx emission of a turbocharged hydrogen internal combustion engine. Int J Hydrogen Energy 5573–5584 2019. https://doi.org/10.1016/j.ijhydene.2018.08.184.
[5] Du H, Chai WS, Wei H, Zhou L. Status and challenges for realizing low emission with hydrogen ultra-lean combustion. Int J Hydrogen Energy 2024;57:1419–36. https://doi.org/10.1016/j.ijhydene.2024.01.108.
[6] Valente A, Iribarren D, Candelaresi D, Spazzafumo G, Dufour J. Using harmonised life-cycle indicators to explore the role of hydrogen in the environmental performance of fuel cell electric vehicles. Int J Hydrogen Energy 2020;45(47):25758–65. https://doi.org/10.1016/j.ijhydene.2019.09.059.
[7] Arnd Franz, Opportunities and Challenges on the Way to a Hydrogen Mobility, 45th International Vienna Motor Symposium 24 - 26 April 2024, 2024, doi:10.62626/7fuy-6j4x.
[8] J. L. Beduneau, L. Doradoux, G. Meissonnier, M. Da Graca, Y. Rimlinger, G. Dober, B. Gomot, and W. F. Piock, Powertrains for High Intensity Applications – 24 Hours with H2ICE, 45th International Vienna Motor Symposium 24 - 26 April 2024, 2024, doi:10.62626/wiwh-4y3g.
[9] Pulvirenti L, Rolando L, Vinogradov A, Peiretti Paradisi B. Comparison of hydrogen-fueled powertrains for urban bus applications — design, modeling, and energy management. Int J Hydrogen Energy 2024;110:560–74. https://doi.org/10.1016/j.ijhydene.2025.02.004.
[10] Millo F, Rolando L, Fuso R, Zhao J. Development of a new hybrid bus for urban public transportation. Appl Energy 2015;157:583–94. https://doi.org/10.1016/j.apenergy.2015.03.131.
[11] Brancaleoni PP, Damiani Ferretti AN, Corti E, Ravaglioli V, Moro D. Lifecycle CO2 analysis for urban emission reduction of hydrogen-fuelled and battery electric buses in the European Union current and future energetic scenarios. Int J Hydrogen Energy 2025;123:335–53. https://doi.org/10.1016/j.ijhydene.2025.03.397.
[12] Peiretti Paradisi B, Pulvirenti L, Prussi M, Rolando L, Vinogradov A. Life cycle assessment of different powertrain alternatives for a clean urban bus across diverse weather conditions. Energies 2025;18(17). https://doi.org/10.3390/en18174522.
[13] Peiretti Paradisi B, Pulvirenti L, Vinogradov A, Rolando L, Piano A, Millo F, et al. A techno-economic life cycle assessment of H2 fuelled and electrified urban buses. Appl Energy 2025;401. https://doi.org/10.1016/j.apenergy.2025.126738.
[14] Göhlich D, Fay TA, Jefferies D, Lauth E, Kunith A, Zhang X. Design of urban electric bus systems. Des Sci 2018;4. https://doi.org/10.1017/dsj.2018.10.
[15] HyFLEET:CUTE, Hydrogen Transport, Bus Technology & Fuel for today and for a Sustainable Future; Jul. 2023. https://trimis.ec.europa.eu/sites/default/files/project/documents/20121019_155212_90810_HyFLEETCUTE_Brochure_Web.pdf.
[16] Chandler K. SunLine transit agency hydrogen-powered transit buses. Third Evaluation Report and Appendices 2008.
[17] Arsie I, Battistoni M, Brancaleoni PP, Cipollone R, Corti E, Di Battista D, Millo F, Occhicone A, Peiretti Paradisi B, Rolando L, Zembi J. A new generation of hydrogen-fueled hybrid propulsion systems for the urban mobility of the future. Energies 2024;17(1). https://doi.org/10.3390/en17010034.
[18] Kivekäs, K., Lajunen, A., Vepsäläinen, J., and Tammi, K., City bus powertrain comparison: Driving cycle variation and passenger load sensitivity analysis, Energies. 11(7), 2018, doi:10.3390/en11071755.
[19] Transport for London, London exhaust emissions study: A summary of the drive cycle development, test programme and comparison of test data compared with type approval data, http://content.tfl.gov.uk/london-exhaust-emissions-study-drive-cycle-development.pdf, 2020.
[20] Vassallo, A., Pesce, F., Arpaia, A., Millo, F., Rolando, L., Piano, A., and Bianco, A., Ultra-lean Combustion System Optimization for H2-fuelled ICEs via Synergistic Application of 1D- and 3D-CFD, SIA POWERTRAIN & POWER ELECTRONICS, Digital Edition 2021, 1–9.
[21] Golisano R, Scalabrini S, Arpaia A, Pesce F, Vassallo A, Borgia F, et al. Hydrogen internal combustion engine & KERS: an appealing value-proposition for green power pack. 42nd International Vienna Motor Symposium. 2021.
[22] Millo F, Piano A, Rolando L, Accurso F, Gullino F, Roggio S, Bianco A, Pesce F, Vassallo A, Rossi R. Synergetic application of zero-, one-, and three-dimensional computational fluid dynamics approaches for hydrogen-fuelled spark ignition engine simulation. SAE Int J Engines 2021;15(4). https://doi.org/10.4271/03-15-04-0030.
[23] Rahantamialisoa FNZ, Zembi J, Miliozzi A, Sahranavardfard N, Battistoni M. CFD simulations of under-expanded hydrogen jets under high-pressure injection conditions. Journal of Physics: Conference Series Institute of Physics 2022. https://doi.org/10.1088/1742-6596/2385/1/012051.
[24] Gammaidoni T, Miliozzi A, Zembi J, Battistoni M. Hydrogen mixing and combustion in an SI internal combustion engine: CFD evaluation of premixed and DI strategies. Case Stud Therm Eng 2024;55. https://doi.org/10.1016/j.csite.2024.104072.
[25] Rahantamialisoa F, Battistoni M, Miliozzi A, Sahranavardfard N, Zembi J. Investigations on hydrogen injections using a real-fluid approach. SAE Technical Paper 2023-01-0312 2023. https://doi.org/10.4271/2023-01-0312.
[26] Merola SS, Irimescu A, DiIorio S, Vaglieco BM. Effect of fuel injection strategy on the carbonaceous structure formation and nanoparticle emission in a disi engine fuelled with butanol. Energies 2017;10(7). https://doi.org/10.3390/en10070832.
[27] Ricci F, Mariani F, Papi S, Zembi J, Battistoni M, Grimaldi CN. The synergy between methanol M100 and plasma-assisted ignition system PAI to achieve increasingly leaner mixtures in a single-cylinder engine. Energies 2024;17(7). https://doi.org/10.3390/en17071659.
[28] Azeem N, Beatrice C, Vassallo A, Pesce F, Davide G, Guido C, et al. Comparative analysis of different methodologies to calculate lambda (λ) based on extensive and systemic experimentation on a hydrogen internal combustion engine. SAE Technical Papers 2023-01-0340 2023. https://doi.org/10.4271/2023-01-0340.
[29] Ricci F, Zembi J, Avana M, Grimaldi CN, Battistoni M, Papi S. Analysis of hydrogen combustion in a spark ignition research engine with a barrier discharge igniter. Energies 2024;17(7). https://doi.org/10.3390/en17071739.
[30] Hires SD, Tabaczynski RJ, Novak JM. The prediction of ignition delay and combustion intervals for a homogeneous charge, spark ignition engine. SAE Technical Paper 1979;780232. https://doi.org/10.4271/780232.
[31] Morel T, Rackmil CI, Keribar R, Jennings MJ. Model for heat transfer and combustion in spark ignited engines and its comparison with experiments. SAE Technical Paper 1988;880198. https://doi.org/10.4271/880198.
[32] Zhao J, Xu M. Fuel economy optimization of an Atkinson cycle engine using genetic algorithm. Appl Energy 2013;105:335–48. https://doi.org/10.1016/j.apenergy.2012.12.061.
[33] Zembi J, Cruccolini V, Mariani F, Scarcelli R, Battistoni M. Modeling of thermal and kinetic processes in non-equilibrium plasma ignition applied to a lean combustion engine. Appl Therm Eng 2021;197. https://doi.org/10.1016/j.applthermaleng.2021.117377.

[34] Zembi J, Battistoni M, Nambully SK, Pandal A, Mehl C, Colin O. LES investigation of cycle-to-cycle variation in a SI optical access engine using TFM-AMR combustion model. Int J Engine Res 2022;23(6):1027–46. https://doi.org/10.1177/14680874211005050.
[35] Zembi J, Mariani F, Battistoni M. Large eddy simulation of ignition and combustion stability in a lean SI optical access engine. SAE Technical Papers 2019-24-0087 2019. https://doi.org/10.4271/2019-24-0087.
[36] Dong S, Wagnon SW, Pratali Maffei L, Kukkadapu G, Nobili A, Mao Q, et al. A new detailed kinetic model for surrogate fuels: C3MechV3.3. Appl Energy Combust Sci 2022;9. https://doi.org/10.1016/j.jaecs.2021.100043.
[37] Peters N., Turbulent Combustion, ISBN0-521-66082-3., 2000.
[38] Zembi J, Battistoni M, Mariani F, Irimescu A, Vaglieco BM, Merola SS. Investigations on the impact of port water injection on soot formation in a DISI engine through CFD simulations and optical methods. Fuel 2023;337. https://doi.org/10.1016/j.fuel.2022.127170.
[39] Heywood JB. Internal Combustion Engine Fundamentals, New York :McGraw-Hill Book Company 1988.
[40] Ricci F, Avana M, Mariani F. Artificial neural networks as a tool for high-accuracy prediction of in-cylinder pressure and equivalent flame radius in hydrogen-fueled internal combustion engines. Energies 2025;18(2). https://doi.org/10.3390/en18020299.
[41] Maroteaux F, Sebai S, Mancaruso E, Rossetti S, Schembri P, Radja K, et al. Numerical and experimental analysis of dual fuel hydrogen/diesel combustion at varying engine speed on a single cylinder engine. SAE Technical Papers 2024-24-0044 2024. https://doi.org/10.4271/2024-24-0044.
[42] Avana, M., Ricci, F., Papi, S., Zembi, J., Battistoni, M., and Grimaldi, C.N., Performance Analysis of Hydrogen Combustion under Ultra Lean Conditions in a Spark Ignition Research Engine Using a Barrier Discharge Igniter, SAE Int. J. Adv. & Curr. Prac. in Mobility 7(3):1424-1436, 2025, 2024, doi:10.4271/2024-24-0036.
[43] Di Prospero F, Di Battista D, Cipollone R. Model based design of a turbo-compound bottomed to internal combustion engine exhaust gas. Journal of Physics: Conference Series Institute of Physics 2024. https://doi.org/10.1088/1742-6596/2893/1/012095.
[44] Brancaleoni PP, Corti E, Di Prospero F, Di Battista D, Cipollone R, Ravaglioli V. Optimization of hydrogen internal combustion engines equipped with turbocompound technology for enhanced performance and efficiency. Energies 2025;18(9). https://doi.org/10.3390/en18092166.
[45] Rosset K, Pajot O, Schiffmann J. Experimental investigation of a small-scale organic rankine cycle turbo-generator supported on gas-lubricated bearings. J Eng Gas Turbine Power 2021;143(5). https://doi.org/10.1115/1.4049988.
[46] Fatigati F, DiBattista D, Cipollone R. Permeability effects assessment on recovery performances of small-scale ORC plant. Appl Therm Eng 2021:196. https://doi.org/10.1016/j.applthermaleng.2021.117331.
[47] Fatigati F, Vittorini D, Wang Y, Song J, Markides CN, Cipollone R. Design and operational control strategy for optimum off-design performance of an ORC plant for low-grade waste heat recovery. Energies 2020;13(21). https://doi.org/10.3390/en13215846.
[48] Fatigati F, Di Battista D, Carapellucci R. Model-based assessment of a feedforward-feedback control strategy for ORC-based unit in waste heat recovery application. Appl Therm Eng 2025;258. https://doi.org/10.1016/j.applthermaleng.2024.124774.
[49] DiBattista D., Diomede D., Di Prospero F., Bartolomeo M., Cipollone R., Carapellucci R. Turbocompound energy recovery option on a turbocharged diesel engine, I talian thermal machines conference. Carpi, Modena ; 2023.
[50] Di Battista D, Di Prospero F, Di Giovine G, Fatigati F, Cipollone R. Dual-stage energy recovery from internal combustion engines. Energies 2025;18(3). https://doi.org/10.3390/en18030623.
[51] Di Battista D, Mauriello M, Cipollone R. "Effects of an ORC based heat recovery system on the performances of a diesel engine". SAE Technical Papers 2015-01-1608 2015. https://doi.org/10.4271/2015-01-1608.
[52] Di Battista D, Bartolomeo MD, Villante C, Cipollone R. A model approach to the sizing of an ORC Unit for WHR in transportation sector. SAE Int J Commer Veh 2017;10(2):608–17. https://doi.org/10.4271/2017-24-0159.
[53] Muhammad Farhan S, Pan W, Zhijian C, JianJun Y. Innovative catalysts for the selective catalytic reduction of NOx with H2: a systematic review. Fuel 2024;355. https://doi.org/10.1016/j.fuel.2023.129364.
[54] Guan Y, Liu Y, Lv Q, Wang B, Che D. Review on the selective catalytic reduction of NOx with H2 by using novel catalysts. J Environ Chem Eng 2021;9(6). https://doi.org/10.1016/j.jece.2021.106770.
[55] Crispi M. R., Occhicone A., Cortabitarte C. C., Arsie I., Roviello G. Experimental investigation of innovative H2-SCR systems for NOx abatement in hydrogen-fueled ICEs. Submitted to Fuel 2025.
[56] Raad Z, Toufaily J, Hamieh T, Domine ME. Tio2-supported pd as an efficient and stable catalyst for the mild hydrotreatment of tar-type compounds. Nanomaterials 2021;11(9). https://doi.org/10.3390/nano11092380.
[57] Zhang J, Alexandrova AN. Structure, stability, and mobility of small Pd clusters on the stoichiometric and defective TiO2 (110) surfaces. J Chem Phys 2011;135(17). https://doi.org/10.1063/1.3657833.
[58] Han X, Zhang L, Zhang R, Wang K, Wang X, Li B, et al. Boosting the catalytic performance of Al2O3-supported Pd catalysts by introducing CeO2 promoters. Dalton Trans 2024;53(7):3290–5. https://doi.org/10.1039/d3dt03676f.
[59] Brancaleoni PP, Corti E, Ravaglioli V, Moro D, Silvagni G. Innovative torque-based control strategy for hydrogen internal combustion engine. Int J Hydrogen Energy 2024;73:203–20. https://doi.org/10.1016/j.ijhydene.2024.05.481.
[60] Brancaleoni PP, Corti E, Ravaglioli V, Moro D, Silvagni G, Brusa A, et al. Performance evaluation of hydrogen-powered internal combustion engine city bus for the urban mobility of Bologna, Italy. Journal of Physics: Conference Series Institute of Physics 2024. https://doi.org/10.1088/1742-6596/2893/1/012068.
[61] Ravaglioli V, Silvagni G, Ponti F, et al. Development of a control-oriented physical model for cylinder pressure peak estimation in SI engines. Int J Engine Res 2025;26. https://doi.org/10.1177/14680874241272904.
[62] Brancaleoni PP, Corti E, Silvagni G, Ravaglioli V. Physical-based peak pressure controller for hydrogen internal combustion engines. Int J Hydrogen Energy 2025;133:377–85. https://doi.org/10.1016/j.ijhydene.2025.04.457.
[63] Corti E, Abbondanza M, Ponti F, Raggini L. The use of piezoelectric washers for feedback combustion control. SAE Technical Papers 2020-01-1146 2020. https://doi.org/10.4271/2020-01-1146.
[64] Onori S, Serrao L, Rizzoni G. Hybrid electric vehicles. Energy management strategies, Springer 2016.
[65] Nacci G, Cervone D, Frasci E, Lakshmanan VK, Sciarretta A, Arsie I. EMS optimization of a series-hybrid urban bus with hydrogen-fueled engine accounting for NOx emissions and eco-driving. SAE Technical Papers 2024-24-0009 2024. https://doi.org/10.4271/2024-24-0009.
[66] Xing X, Wan L, Luo F. Demand prediction for shared bicycles around metro stations incorporating STAGCN. PLoS One 20(7 July) 2025. https://doi.org/10.1371/journal.pone.0328452.
[67] The MathWorks, Inc., Simulink version R2024,https://www.mathworks.com/products/simulink.html, 2024.
[68] UITP – International Association of Public Transport. SORT – Standardize On-Road Test Cycle. https://www.uitp.org/publications/uitp-sort-e-sort-brochures/.2004.
[69] Dornoff J, Rodríguez F. Euro 7: the new emission standard for light- and heavy-duty vehicles in the European Union. ICCT Policy Update 2024.